

# Single and Dual Vector Gene Therapy with AAV9-PHP.B Rescues Hearing in *Tmc1* Mutant Mice

Jason Wu,<sup>1,4</sup> Paola Solanes,<sup>2,4</sup> Carl Nist-Lund,<sup>1,4</sup> Sofia Spataro,<sup>2</sup> Olga Shubina-Oleinik,<sup>1</sup> Irina Marcovich,<sup>1</sup> Hannah Goldberg,<sup>1</sup> Bernard L. Schneider,<sup>2,3,5</sup> and Jeffrey R. Holt<sup>1,5</sup>

<sup>1</sup>Departments of Otolaryngology and Neurology, Boston Children's Hospital and Harvard Medical School, Boston, MA 02115, USA; <sup>2</sup>Brain Mind Institute, Ecole Polytechnique Fédérale de Lausanne, Station 19, 1015 Lausanne, Switzerland; <sup>3</sup>Bertarelli Foundation Gene Therapy Platform, Ecole Polytechnique Fédérale de Lausanne, Ch. des Mines 9, 1202 Geneva, Switzerland

**AAV-mediated gene therapy is a promising approach for treating genetic hearing loss. Replacement or editing of the *Tmc1* gene, encoding hair cell mechanosensory ion channels, is effective for hearing restoration in mice with some limitations. Efficient rescue of outer hair cell function and lack of hearing recovery with later-stage treatment remain issues to be solved. Exogenous genes delivered with the adeno-associated virus (AAV)9-PHP.B capsid via the utricle transduce both inner and outer hair cells of the mouse cochlea with high efficacy. Here, we demonstrate that AAV9-PHP.B gene therapy can promote hair cell survival and successfully rescues hearing in three distinct mouse models of hearing loss. *Tmc1* replacement with AAV9-PHP.B in a *Tmc1* knockout mouse rescues hearing and promotes hair cell survival with equal efficacy in inner and outer hair cells. The same treatment in a recessive *Tmc1* hearing-loss model, *Baringo*, partially recovers hearing even with later-stage treatment. Finally, dual delivery of *Streptococcus pyogenes* Cas9 (SpCas9) and guide RNA (gRNA) in separate AAV9-PHP.B vectors selectively disrupts a dominant *Tmc1* allele and preserves hearing in *Beethoven* mice, a model of dominant, progressive hearing loss. *Tmc1*-targeted gene therapies using single or dual AAV9-PHP.B vectors offer potent and versatile approaches for treating dominant and recessive deafness.**

## INTRODUCTION

Congenital hearing loss is a major health issue affecting 1 in 500 newborns, having a profound impact on early speech and language acquisition, which often affects social development and extends throughout adult life.<sup>1,2</sup> More than 50% of congenital hearing-loss cases have a genetic basis,<sup>3</sup> accounting for ~60% of all deafness over the course of a lifetime.<sup>1</sup> Due to the direct surgical accessibility of the cochlea, as well as its relatively contained fluid environment, gene therapy is a promising approach for treatment of sensory hearing loss. In recent years, a few studies have approached gene therapy for hearing loss<sup>4</sup> with strategies including gene replacement with adeno-associated viruses (AAVs),<sup>5–7</sup> gene suppression with antisense oligonucleotides and

RNA interference,<sup>8,9</sup> and gene and base editing with CRISPR-Cas9-based tools.<sup>10,11</sup>

A number of gene-therapy studies have targeted the *Tmc1* gene, which encodes a mechanosensitive ion channel in hair cells of the inner ear and mediates the conversion of mechanical stimulation from sound into electrical signals for hearing sensation.<sup>12–14</sup> Mutations in *Tmc1* cause dominant DFNA36, and recessive DFNB7/11, deafness<sup>15</sup> and lead to 3%–8% of all inherited hearing-loss conditions.<sup>16</sup> TMC1 is located at the tips of stereocilia of inner hair cells (IHCs) and outer hair cells (OHCs), two types of sensory cells of the inner ear. In mice, the lack of functional TMC1 results in loss of mechanosensory transduction, profound hearing deficits, and hair cell death.<sup>13,17</sup> Hair cells are organized in a tonotopic gradient along the organ of Corti, transducing high frequencies at the base and low frequencies at the apex. IHCs are responsible for signal transduction to afferent type I spiral ganglion neurons and transmission to the brain, whereas OHCs are necessary to amplify and tune the response to sound stimuli.

In mouse models of hearing loss, lack of mechanosensory transduction causes hair cell death, which progresses from the base to apex, with OHCs degenerating earlier than IHCs. Prior reports of partial hearing restoration using viral-mediated gene therapy coincide with levels of hair cell survival.<sup>5,11</sup> One major challenge that must be addressed with developing AAV tools for hearing loss is understanding how to effectively minimize this spatiotemporal pattern of degeneration. This requires efficient and specific viral transduction into both IHCs and OHCs, as well as a sufficiently broad therapeutic window for exogenous gene expression in surviving hair cells.

Received 4 August 2020; accepted 11 November 2020;  
<https://doi.org/10.1016/j.ymthe.2020.11.016>

<sup>4</sup>These authors contributed equally

<sup>5</sup>Senior author

**Correspondence:** Jeffrey R. Holt, Departments of Otolaryngology and Neurology, Boston Children's Hospital and Harvard Medical School, Boston, MA 02115, USA.  
**E-mail:** [jeffrey.holt@childrens.harvard.edu](mailto:jeffrey.holt@childrens.harvard.edu)



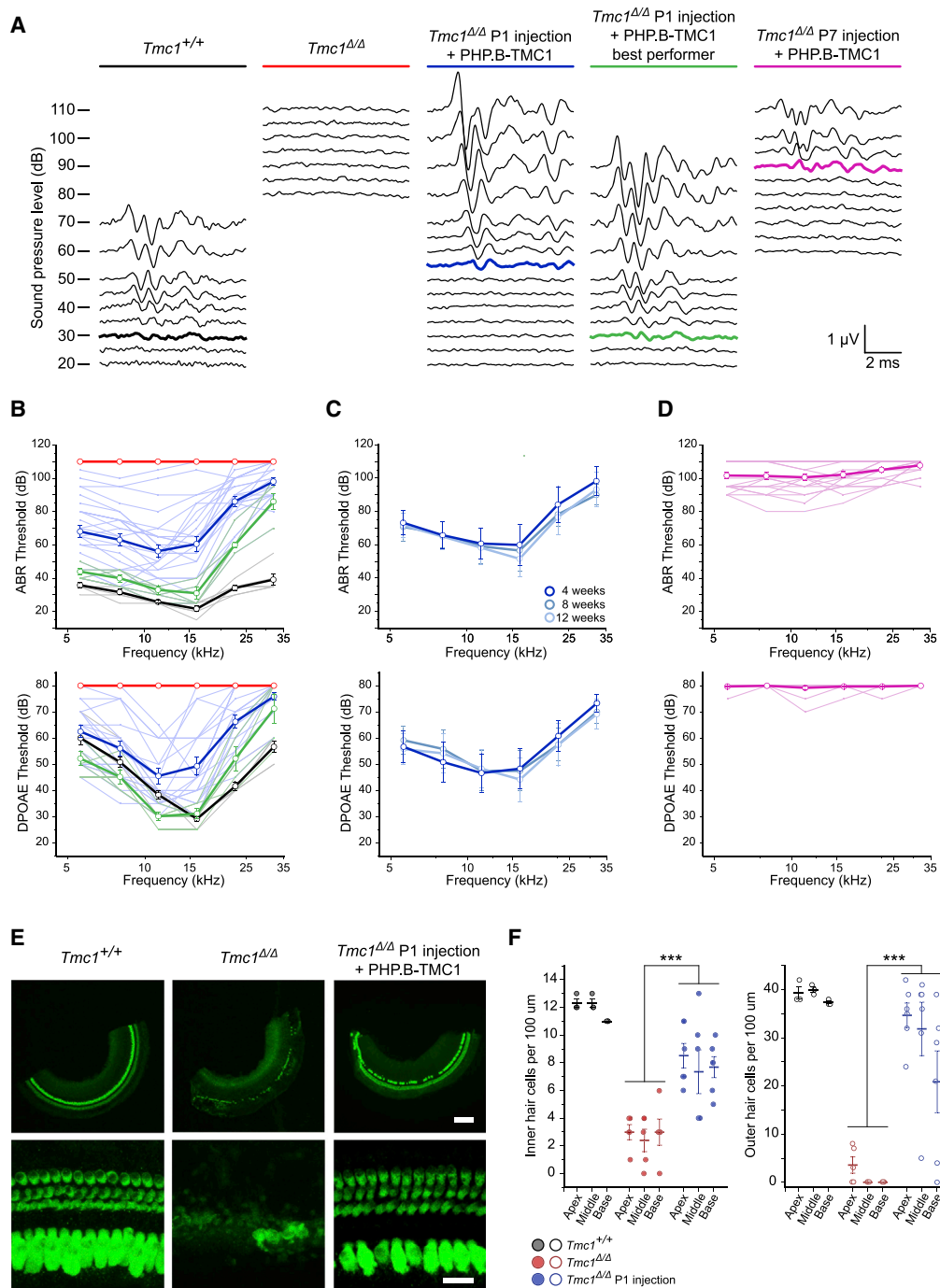


**Figure 1. AAV2/9-PHP.B-Tmc1 Mediates Hearing Restoration in  $Tmc1^{\Delta/\Delta}$  Mice**

(A) Representative ABR waveform families recorded from mice at 4 weeks or 4 weeks postinjection for each indicated condition, using 11.3 kHz tone bursts at incrementally increasing sound-pressure levels. Thresholds were determined by the detection of peak 1 and are indicated by colored traces. Scale bar applies to all families. (B) Mean ABR (top) and DPOAE (bottom) thresholds of 4-week-old mice plotted as a function of stimulus frequency for wild-type (WT) C57BL/6 (black;  $n = 6$ ),  $Tmc1^{\Delta/\Delta}$  uninjected controls (red;  $n = 5$ ), and  $Tmc1^{\Delta/\Delta}$  mice injected with PHP.B-Tmc1 at P1 (blue;  $n = 28$ ) with five best performers (green) tested at 4 weeks old. Lighter traces show individual responses. Average data shown as mean  $\pm$  SEM. (C) Mean ABR (top) and DPOAE (bottom) thresholds plotted as a function of stimulus frequency for  $Tmc1^{\Delta/\Delta}$  mice injected with PHP.B-Tmc1 at P1, tested at 4, 8, and 12 weeks after injection ( $n = 6$ ). Average data shown as mean  $\pm$  SEM. (D) Mean ABR (top) and DPOAE (bottom) thresholds plotted as a function of stimulus frequency for  $Tmc1^{\Delta/\Delta}$  mice injected with PHP.B-Tmc1 at P7, tested at 4 weeks after injection ( $n = 19$ ). Lighter traces show individual responses. Average data shown as mean  $\pm$  SEM. (E) Representative 10 $\times$  (top panels) and 63 $\times$  (bottom panels) confocal images from middle-apical cochlear sections of indicated experimental (legend continued on next page)

Recently, the synthetic AAV9-PHP.B capsid was identified to enable enhanced gene transduction in the central nervous system (CNS) following intravenous administration.<sup>18</sup> Our lab found that AAV9-PHP.B, when combined with an injection directly into the utricle, an inner-ear vestibular organ, was able to transduce both IHCs and OHCs along the entire length of the cochlea with near-100% efficacy even when injected at later postnatal ages.<sup>19</sup> This demonstrates a notable improvement from other tested capsids and previous studies in which OHC transduction was limited, and transduction efficacy in IHCs decreased from apex to base.<sup>19,20</sup> Additionally, two other studies showed that round window membrane administration of AAV9-PHP.B allows for near-complete transduction of hair cells in nonhuman primates as well.<sup>6,21</sup> One of these studies also used AAV9-PHP.B to deliver CLRN1 to a mouse model of Usher syndrome type 3A and demonstrated moderate hearing restoration.<sup>6</sup>

Here, we sought to characterize the extent of hearing recovery in three different *Tmc1*-deficient mouse models for hearing loss with the use of AAV9-PHP.B delivery via the utricle. We tested the efficacy of *Tmc1* gene replacement in two different forms of recessive hearing loss, as well as the efficacy of dual vector delivery of a CRISPR-Cas9 system to treat a form of dominant hearing loss. Due to the unprecedented efficacy of viral transduction in hair cells using AAV9-PHP.B, we hypothesized that we would see improved recovery of hearing and decreased levels of cell death.

We found that AAV9-PHP.B was able to effectively induce transgenic expression or modify native genes in hair cells and prevent hearing loss for all three mouse strains tested, in some cases, to a greater extent than previously reported with other AAV strategies. Additionally, we found that treatment at older ages in different mouse strains revealed possible limitations to gene therapy in hair cells. Finally, we demonstrated that AAV9-PHP.B enables robust dual vector delivery, thus expanding the tool kit for AAV-based gene therapy.

## RESULTS

### PHP.B-Tmc1 Mediates Hearing Restoration in *Tmc1*<sup>Δ/Δ</sup> Mice

Restoration of hearing in mouse models for congenital hearing loss has been explored with the use of AAV-mediated gene delivery.<sup>5,6,10,11,20,22</sup> Notably, our group has recently demonstrated that delivery of *Tmc1* with the synthetic AAV-Anc80L65 capsid can restore hearing in a mouse model for human recessive deafness DFNB7/11, in some cases, to near-wild-type (WT) thresholds of hearing.<sup>5</sup> Additionally, we have also recently reported that the AAV9-PHP.B capsid, delivered through a novel injection route to the utricle, can transduce nearly 100% of both IHCs and OHCs throughout all cochlear turns with EGFP, even when injected as late as postnatal day 7 (P7).<sup>19</sup> Here, we asked if a combination of these strategies could

yield an even more robust recovery of hearing in a *Tmc1*<sup>Δ/Δ</sup> mouse line, a model of DFNB7/11.

To address this question, we packaged mouse *Tmc1ex1* driven by the cytomegalovirus (CMV) promoter and followed by a woodchuck hepatitis virus (WHP) post-transcriptional regulatory element (WPRE) sequence into the AAV9-PHP.B capsid: AAV2/9-PHP.B-CMV-TMC1-WPRE (PHP.B-Tmc1 for brevity). We then injected 1 μL (5.64E+10 gc) into the left utricle of P1 *Tmc1*<sup>Δ/Δ</sup> mice. After 4 weeks, we recorded auditory brainstem responses (ABRs) and distortion product otoacoustic emissions (DPOAEs) from injected and uninjected mice to evaluate the extent of hearing recovery across frequencies ranging from 5.6 kHz to 32 kHz.

At P28–P30, *Tmc1*<sup>Δ/Δ</sup> mice were profoundly deaf, with no recorded ABRs or DPOAEs evoked by up to 110 decibels (dB) or 80 dB sound-pressure level (SPL), respectively (Figures 1A and 1B). PHP.B-Tmc1-injected mice, however, showed significant hearing recovery, with an ~60-dB SPL average auditory threshold across tested frequencies (at 11.3 kHz, *Tmc1*<sup>Δ/Δ</sup>: 110 ± 0 dB, n = 5; injected: 56.3 ± 3.8 dB, n = 28) (Figures 1A and 1B). The five best performers out of 28 injected mice, identified by mean ABR threshold across all frequencies, recovered hearing thresholds as low as 20–40 dB, similar to those of WT C57BL/6 mice (at 11.3 kHz, WT: 25.8 ± 0.8 dB, n = 6; injected: 31.0 ± 1.9 dB, n = 5) (Figures 1A and 1B). Recovery at higher frequencies was more modest and is consistent with the more rapid degradation of hair cells toward the basal turn of the cochlea in mouse models for hearing loss (Figure 1B). DPOAEs, a measure of OHC function, recorded from injected mice, were, on average, nearly indistinguishable from WT mice at low frequencies up to 11.3 kHz and showed substantial improvements at higher frequencies compared to previous reports of gene-therapy strategies for hearing loss (at 11.3 kHz, *Tmc1*<sup>Δ/Δ</sup>: 80 ± 0 dB n = 5; injected: 45.5 ± 3.0 dB, n = 28) (Figure 1B). The five best performers had DPOAE thresholds near or equal to those of WT mice across all frequencies (at 11.3 kHz, WT: 38.3 ± 1.7 dB, n = 6; injected: 30.0 ± 1.6 dB, n = 5) (Figure 1B). Additionally, recovery of both ABRs and DPOAEs was robust when mice were tested 8 and 12 weeks following injection, demonstrating the long-term durability of this gene-delivery strategy (ABRs at 11.3 kHz, 4 weeks: 59.2 ± 10.4 dB; 8 weeks: 58.3 ± 10.0 dB; 12 weeks: 60.8 ± 9.3 dB, n = 6) (Figure 1C).

Previously, we observed that injection of AAV-Anc80L65-Tmc1 at later ages resulted in progressively less effective recovery of hearing, as the postnatal injection age increased.<sup>5</sup> Because we have shown that the AAV9-PHP.B capsid can efficiently transduce EGFP in hair cells of P7 C57BL/6 WT mice, we asked if delivery of *Tmc1* using PHP.B-Tmc1 could improve hearing recovery at later injection time points. When injected at P7 and measured 4 weeks postinjection, 12/19

conditions, immunostained against myosin VIIa at 12 weeks of age. Scale bars, 100 μm at 10× and 20 μm at 63×. (F) Mean cell counts of inner (left) and outer (right) hair cells (IHCs and OHCs, respectively) for WT C57BL/6 (n = 3), *Tmc1*<sup>Δ/Δ</sup> uninjected controls (n = 5), and P1-injected *Tmc1*<sup>Δ/Δ</sup> conditions (n = 6) at 12 weeks of age measured from 100 μm sections of the apex, middle, and basal cochlear turns. Individual samples are shown as a scatterplot (\*\*p ≤ 0.001; one-way ANOVA followed by Sidak's multiple comparison test for respective measurements, i.e., *Tmc1*<sup>Δ/Δ</sup> apex versus injected apex).

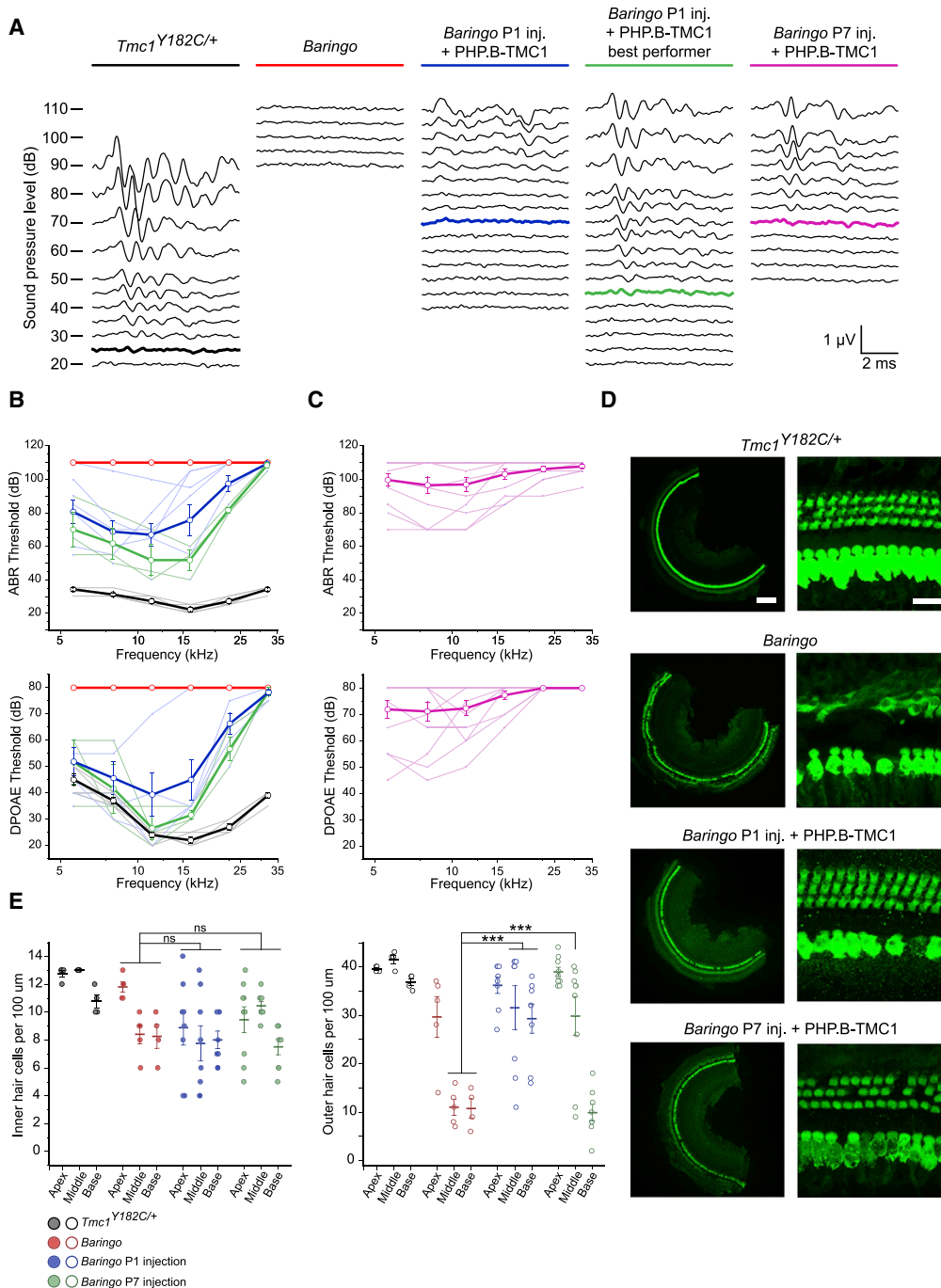


**Figure 2. AAV9-PHP.B-Mediated Hearing Recovery in the Recessive Hearing-Loss Model, *Baringo***

(A) Representative ABR waveform families recorded from mice at 4 weeks or 4 weeks postinjection for indicated conditions, using 11.3 kHz tone bursts at incrementally increasing sound-pressure levels. Thresholds were determined by the detection of peak 1 and are indicated by colored traces. Scale bar applies to all families. (B) Mean ABR (top) and DPOAE (bottom) thresholds of 4-week-old mice plotted as a function of stimulus frequency for *Tmc1*<sup>Y182C/+</sup> (black; n = 5), *Baringo* uninjected controls (red; n = 4), and *Baringo* mice injected with PHP.B-Tmc1 at P1 (blue; n = 8) with three best performers (green) tested at 4 weeks old. Lighter traces show individual responses. Average data shown as mean  $\pm$  SEM. (C) Mean ABR (top) and DPOAE (bottom) thresholds plotted as a function of stimulus frequency for *Baringo* mice injected with PHP.B-Tmc1 at P7, tested at 4 weeks after injection (n = 13). Lighter traces show individual responses. Average data shown as mean  $\pm$  SEM. (D) Representative 10 $\times$  (left panels) and 63 $\times$  (right panels) confocal images from middle-apical cochlear sections of indicated experimental conditions, immunostained against myosin VIIa at 4 weeks of age or 4 weeks

(legend continued on next page)

mice showed very modest levels of hearing recovery measured by ABR, averaging ~100 dB thresholds, with the best performer reaching 80 dB thresholds at higher frequencies (at 11.3 kHz,  $100.5 \pm 2.2$  dB,  $n = 19$ ) (Figure 1D). DPOAEs were detected in only 3/19 injected mice at 70 dB, a small improvement from earlier studies in which DPOAEs were never detected at P7 and older injections (at 11.3 kHz,  $79.2 \pm 0.6$  dB,  $n = 19$ ) (Figure 1D).<sup>5</sup> In contrast, no ABRs or DPOAEs were detected when mice were injected at P14 (data not shown;  $n = 5$ ).

Because hair cells degenerate rapidly over time in *Tmc1*<sup>Δ/Δ</sup> mice<sup>17</sup>, we asked if hair cells lacking TMC1 at later ages presented a cellular state that is less amenable to AAV transduction. We injected AAV2/9-PHP.B-CMV-eGFP-WPRE (PHP.B-EGFP for brevity) in P7 *Tmc1*<sup>Δ/Δ</sup> mice and harvested cochlear tissue 2–4 weeks after injection. We observed that whereas hair cells had begun to degenerate starting at the basal region, EGFP expression was still expressed widely in both IHCs and OHCs throughout all cochlear sections, suggesting that lack of hearing recovery at later age injections was not due to loss of AAV transduction efficacy (Figure S1).

Following ABR and DPOAE measurements, we dissected the organ of Corti from cochleas of tested mice to assess hair cell survival. At 12 weeks old, *Tmc1*<sup>Δ/Δ</sup> mice exhibit substantial loss of both IHCs and OHCs throughout the entire length of the cochlea, with most regions having no surviving hair cells, as identified by immunostaining against the hair cell marker myosin VIIa (Myo7a) and hair cell counts in 100 μm cochlear sections (for apical IHCs, WT:  $12.3 \pm 0.3$  cells,  $n = 3$ , *Tmc1*<sup>Δ/Δ</sup>:  $3.0 \pm 0.6$  cells,  $n = 5$ ; OHCs, WT:  $39.3 \pm 1.3$  cells, *Tmc1*<sup>Δ/Δ</sup>:  $3.6 \pm 1.7$  cells) (Figures 1E and 1F). For mice injected at P1 with PHP.B-Tmc1, cochleas were harvested at 12 weeks of age and showed a significant increase in hair cell survival in both IHCs and OHCs, comparable in some instances to WT levels (for apical IHCs,  $8.5 \pm 0.9$  cells; OHCs,  $34.7 \pm 2.6$  cells,  $n = 6$ ) (Figures 1E and 1F). For OHCs, survival decreased along the length of the cochlea in a gradient fashion toward the basal turn, consistent with previous reports.<sup>5</sup> For P1-injected mice, cochleas harvested at 4 weeks of age had similar levels and patterns of hair cell survival (for apical IHCs,  $10.0 \pm 0.4$  cells; OHCs,  $38.6 \pm 0.7$  cells,  $n = 5$ ) (Figures S2A and S2B).

Mice that were injected at P7 also had substantial IHC survival throughout and OHC survival at the apical cochlear turn when harvested at 4 weeks postinjection (for apical IHCs,  $11.0 \pm 0.2$  cells; OHCs,  $35.7 \pm 1.5$  cells,  $n = 7$ ), despite having little to no hearing recovery at low frequencies (Figure 1D; Figures S2A and S2B). This could be partially explained by the observation that hair cell loss in uninjected *Tmc1*<sup>Δ/Δ</sup> mice is not complete at 4 weeks old, so the number of Myo7a-positive hair cells does not necessarily reflect the number of functional cells at this stage of the disease (Figure S2A). Together, these data show that PHP.B-Tmc1 delivered at P1 through utricle injection

can prevent hair cell loss in *Tmc1*<sup>Δ/Δ</sup> mice and recover hearing, whereas later-stage injections may be insufficient for full hearing recovery despite being able to efficiently transduce hair cells.

### Hearing Recovery with PHP.B-Tmc1 in the Recessive Hearing-Loss Model *Baringo*

Gene-replacement strategies present a promising option for treating recessive forms of hearing loss. The *Baringo* mouse strain harbors a single recessive loss-of-function point mutation (p.Y182C) in *Tmc1* (*Tmc1*<sup>Y182C/Y182C</sup>), while still expressing mutant TMC1 protein in a pattern similar to that of WT.<sup>23</sup> We hypothesized that expression of mutant *Tmc1* as opposed to a complete knockout may form an intact but nonfunctional, mechanosensory complex and provide a more stable and therapeutically relevant setting for introduction of exogenous *Tmc1*, potentially leading to stronger hearing recovery.

Previously, our group used a split cytosine base editor delivered with dual AAV-Anc80L65 vectors to restore high-threshold ABRs in *Baringo* mice but showed no recovery of DPOAEs.<sup>10</sup> Here, we injected PHP.B-Tmc1 into the utricles of P1 *Baringo* mice (*Tmc1*<sup>Y182C/Y182C</sup>). We then measured ABRs and DPOAEs at 4 weeks of age. Heterozygous (Het) mice (*Tmc1*<sup>Y182C/+</sup>) retained normal hearing compared to WT C57BL/6 mice (at 11.3 kHz, ABR:  $27.0 \pm 1.2$  dB; DPOAE:  $24.0 \pm 1.0$  dB,  $n = 5$ ) (Figures 2A and 2B). Uninjected *Baringo* mice had no detectable ABRs or DPOAEs evoked by 110 dB or 80 dB sound intensities, respectively, as reported previously (Figures 2A and 2B).<sup>10</sup> Injected mice, however, had significantly lower ABR thresholds at low to mid frequencies, with the best performers responding at as low as 40 dB, roughly only 10 dB higher than that of TMC1<sup>Y182C/+</sup> mice (at 11.3 kHz, ABR:  $66.9 \pm 6.7$  dB,  $n = 8$ ) (Figures 2A and 2B). Notably, DPOAE thresholds were recovered significantly, with the average three best performers indistinguishable from TMC1<sup>Y182C/+</sup> at 5.6 to 11.3 kHz frequencies (at 11.3 kHz, all mice:  $39.4 \pm 8.2$  dB,  $n = 8$ ; best performers:  $26.7 \pm 4.4$  dB,  $n = 3$ ) (Figure 2B). As with injections in *Tmc1*<sup>Δ/Δ</sup> mice, recovery at higher frequencies was more modest, likely because degradation of hair cells in *Baringo* mice follows a similar temporal and spatial pattern as in *Tmc1*<sup>Δ/Δ</sup>.

Surprisingly, *Baringo* mice injected with PHP.B-Tmc1 at P7 resulted in stronger recovery of both ABR and DPOAE thresholds compared to *Tmc1*<sup>Δ/Δ</sup> mice. 8/13 P7-injected *Baringo* mice recovered ABR thresholds, with multiple mice exhibiting as low as 70 dB at lower frequencies. The most striking difference from P7-injected *Tmc1*<sup>Δ/Δ</sup> mice was observed in DPOAE thresholds. DPOAEs were detected in 6/13 *Baringo* mice injected at P7, with 3 mice having thresholds between 40 and 50 dB at lower frequency stimulations (at 11.3 kHz, ABR:  $96.9 \pm 4.4$  dB; DPOAE:  $72.3 \pm 2.9$  dB,  $n = 13$ ) (Figure 2C). *Baringo* mice injected at P14 had no detectable ABR or DPOAE thresholds (data not shown,  $n = 11$ ).

postinjection. Scale bars, 100 μm at 10× and 20 μm at 63×. (E) Mean cell counts of IHCs (left) and OHCs (right) for *Tmc1*<sup>Y182C/+</sup> ( $n = 4$ ), *Baringo* uninjected controls ( $n = 5$ ), P1-injected *Baringo* ( $n = 9$ ), and P7-injected *Baringo* ( $n = 9$ ) conditions at 4 weeks of age, measured from 100 μm sections of the apex, middle, and basal cochlear turns. Individual samples are shown as a scatterplot (not significant [ $ns$ ]  $\geq 0.05$ , \*\*\* $p \leq 0.001$ ; one-way ANOVA followed by Sidak's multiple comparison test for respective measurements, i.e., *Baringo* apex versus injected apex).

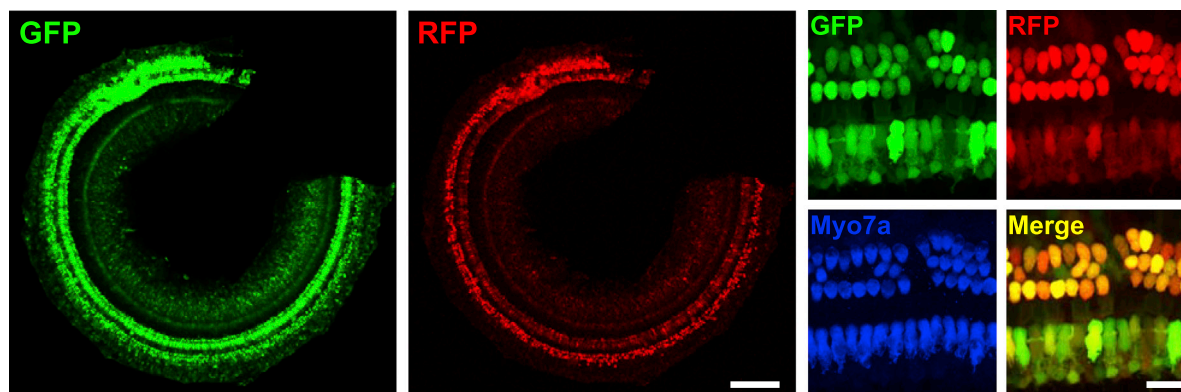


**Figure 3. Coexpression of GFP and RFP by Dual Injection of AAV9-PHP.B Vectors**

Representative 10 $\times$  confocal images (left and middle images) from middle-apical cochlear sections showing GFP (green) and RFP (red) coexpression in IHCs and OHCs. 63 $\times$  magnification of 100  $\mu$ m sections (right images) showing GFP and RFP expression in individual hair cells, merged, and stained against myosin VIIa (blue). Scale bars, 100  $\mu$ m at 10 $\times$  and 20  $\mu$ m at 63 $\times$ .

Following functional testing, we then dissected the organ of Corti and immunostained hair cells of tested mice as before. At 4 weeks of age, we observed modest IHC loss in middle and basal turns of the cochlea in uninjected *Baringo* mice, consistent with prior observations (for middle IHCs, Het:  $13.0 \pm 0$  cells,  $n = 4$ , *Baringo*:  $8.4 \pm 0.7$  cells,  $n = 5$ ; base IHCs, Het:  $10.8 \pm 0.5$  cells, *Baringo*:  $8.3 \pm 0.9$  cells) (Figures 2D and 2E). P1- and P7-injected mice had similarly reduced IHC counts, suggesting that rescue of hearing was mainly due to the reintroduction of functional TMC1 rather than the rescue of hair cell survival (for middle IHCs, P1:  $7.8 \pm 1.3$  cells,  $n = 9$ , P7:  $10.4 \pm 0.3$  cells,  $n = 9$ ; base IHCs, P1:  $8.0 \pm 0.6$  cells, P7:  $7.5 \pm 0.6$  cells) (Figures 2D and 2E). On the other hand, OHCs in uninjected *Baringo* mice were substantially reduced in number in the middle and basal cochlear turns, and remaining hair cells were notably unorganized (for middle OHCs, Het:  $41.5 \pm 0.9$  cells,  $n = 4$ , *Baringo*:  $11.0 \pm 1.6$  cells,  $n = 5$ ; base OHCs, Het:  $36.8 \pm 0.8$  cells, *Baringo*:  $10.8 \pm 2.0$  cells) (Figures 2D and 2E). P1-injected *Baringo* mice had significantly greater OHC survival in the middle and basal cochlear turns, with some mice appearing indistinguishable from *Tmc1*<sup>Y182C/+</sup> (for middle OHCs, P1:  $31.5 \pm 4.5$  cells,  $n = 9$ , P7:  $29.8 \pm 4.0$  cells,  $n = 9$ ; base OHCs, P1:  $29.3 \pm 3.0$  cells, P7:  $9.9 \pm 1.7$  cells) (Figure 2E). Interestingly, P7-injected mice also had a significantly increased survival rate of OHCs in the apical and middle cochlear turns, whereas OHC survival remained low in the basal turn (apical:  $38.9 \pm 0.9$  cells; middle:  $29.8 \pm 4.0$ ; base:  $9.9 \pm 1.7$ ,  $n = 9$ ) (Figure 2E). This observation is in contrast to that seen in P7-injected *Tmc1* <sup>$\Delta/\Delta$</sup>  mice, where there was still substantial hair cell death in the middle cochlear turn. This effect may account for the difference seen in DPOAE thresholds between P7-injected *Tmc1* <sup>$\Delta/\Delta$</sup>  and *Baringo* mice.

#### Coexpression of Different Genes by Dual Injection of AAV9-PHP.B Vectors

Delivery of large gene sequences to the inner ear is limited by the capacity of AAV vectors ( $\leq 5$  kb).<sup>24–26</sup> In addition, many gene-therapy studies require two vectors to deliver multiple genetic elements.<sup>22,24,27</sup>

Whereas dual delivery of large sequences to IHCs has yielded partial success,<sup>22,28</sup> the efficiency of dual delivery to OHCs has been limited.<sup>29</sup> The increased efficacy of gene delivery with AAV9-PHP.B presents an opportunity to improve gene expression of two vectors delivered simultaneously, while being limited by total volume and titer. Perhaps the most impactful of such applications is the delivery of CRISPR-Cas9 systems with AAVs.

To first test the efficacy of dual vector delivery with AAV9-PHP.B, we generated AAV2/9-PHP.B-CMV-turbo red fluorescent protein (RFP)-WPPE (PHP.B-RFP) and coinjected this vector with AAV2/9-PHP.B-CMV-EGFP-WPRE at a 1:1 gc ratio in a total volume of 1  $\mu$ L into the utricle of WT C57BL/6 mice at P1 (1.3E+9 gc each). At P14, mice were harvested, immunostained against Myo7a, and imaged with confocal microscopy for expression of GFP and RFP in hair cells. We observed that among three tested mice, on average, 60% of IHCs and 79% of OHCs coexpressed both GFP and RFP when normalized to total hair cells indicated by Myo7a-positive cells. In one mouse, as high as 93% of IHCs and 90% of OHCs coexpressed both GFP and RFP, although expression level was variable among cells (Figure 3). This result suggests that coinjection of dual AAV9-PHP.B vectors could be a successful strategy for delivering separately encoded elements, such as guide RNA (gRNA) and Cas9 nucleases.

#### Identification of gRNAs Selective for the *Beethoven* (*Bth*) Allele Using the *Streptococcus pyogenes* Cas9 (SpCas9) Nuclease

Recent studies have shown the protective effects of allele-specific RNA-guided nuclease targeting the mutant *Tmc1* gene causing DFNA36-dominant deafness.<sup>11,30</sup> Such an approach has recently been achieved using the KKH variant of SaCas9 nuclease (from *Staphylococcus aureus*) and a gRNA encoded by a single AAV-Anc80L65 vector.<sup>11</sup> The extension of AAV delivery to other nucleases, such as SpCas9, may allow targeting a larger repertoire of genes and mutations. As the coding sequence for SpCas9, gRNA, and promoters

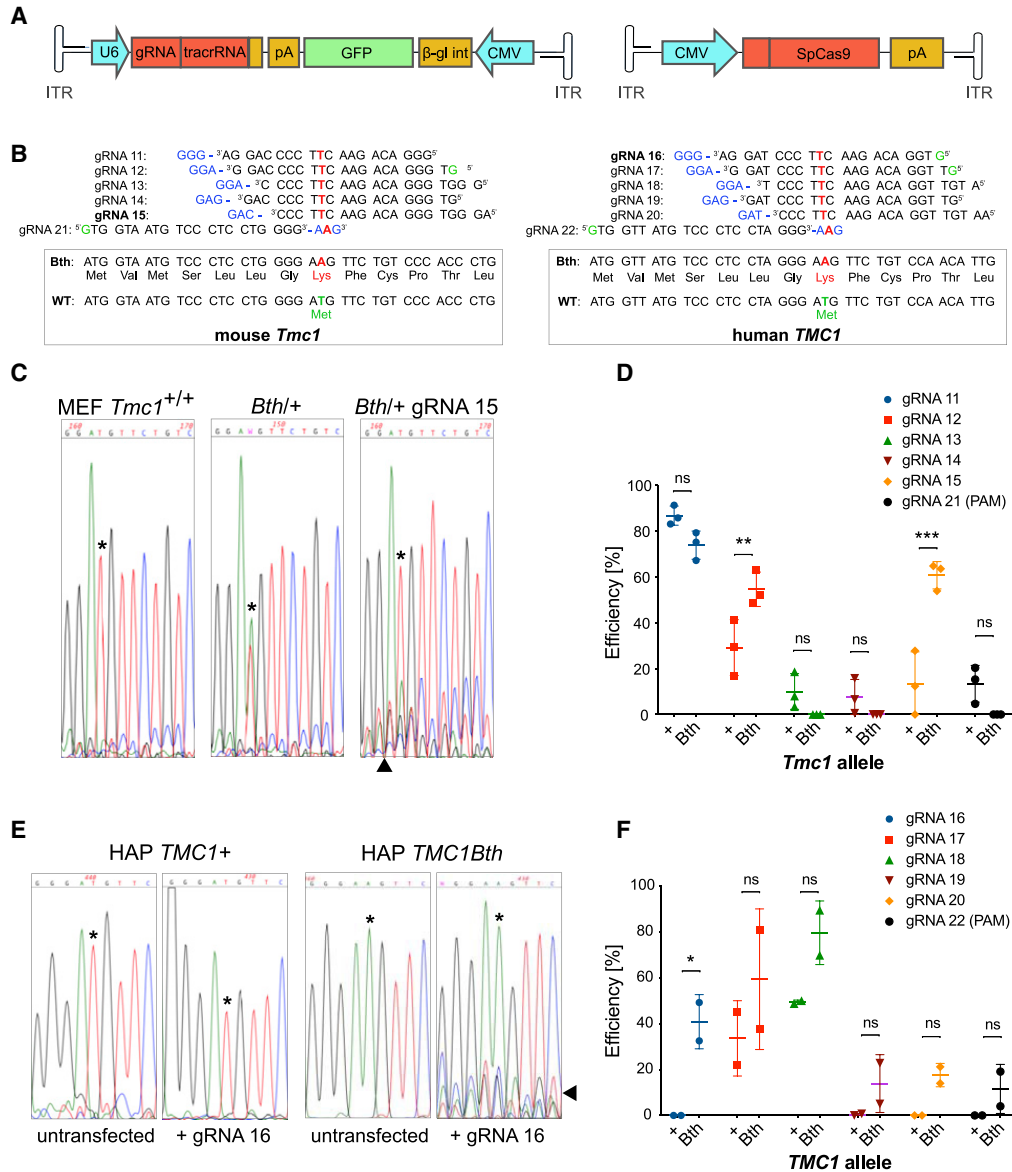


**Figure 4. Screening of gRNAs for Selective Disruption of the *Bth* Allele Mediated by the SpCas9 Nuclease**

(A) Dual AAV vector constructs for expression of the gRNA and SpCas9 nuclease (tracrRNA, *trans*-activating CRISPR RNA; β-glob int, beta-globin intron; pA, 3' UTR and polyadenylation signal; ITR, AAV2-inverted terminal repeats). (B) Design of gRNA sequences targeting the *Bth* mutation. Aligned sequences of the mouse *Tmc1* and human *TMC1* genes are shown in the lower boxes. The PAM sequence is depicted in blue and the nucleotides corresponding to the *Bth* mutation in red. For some gRNA sequences, a G (shown in green) was added to the 5' end to facilitate the activity of the RNA polymerase. (C) Representative sequencing chromatograms of the *Tmc1* gene in MEF cells. Asterisk (\*) indicates the position corresponding to the T-to-A *Bth* point mutation. Note the predominant T in this position in *Bth*<sup>+/+</sup> cells transfected with gRNA 15, which indicates selective SpCas9-mediated cleavage of the *Bth* allele. The arrowhead shows the SpCas9 cleavage site. (D) TIDER quantification of gRNA-induced cleavage efficacy based on the relative presence of the WT or *Bth* sequence in *Bth*<sup>+/+</sup> MEF cells transfected with each of the gRNA-expressing constructs. Note the significant selectivity for the *Bth* allele of gRNA 12 and 15 (ns ≥ 0.05, \*\*p ≤ 0.01, \*\*\*p ≤ 0.001; multiple t tests with Holm-Sidak method). Data shown as mean ± SD. (E) Representative sequencing chromatograms of the *TMC1* gene in HAP *TMC1*<sup>+</sup> and *TMC1*<sup>Bth</sup> cells. Note that indels (arrowhead) are present only in the SpCas9-expressing HAP *TMC1*<sup>Bth</sup> cells transfected with gRNA 16. (F) TIDE analysis of gRNA-induced cleavage efficacy based on indel frequency in HAP cells transfected with each of the gRNA-expressing constructs. Data shown as mean ± SD. Note the significant selectivity of gRNA 16 for the *Bth* allele (\*p ≤ 0.05; multiple t tests with Holm-Sidak method).

exceed the packaging capacity of AAV (≤5 kb), methods based on the coinjection of two AAV vectors separately encoding the gRNA and SpCas9 nuclease need to be optimized.

In order to address this question, we devised a dual AAV system to express SpCas9 and the gRNA using two separate AAV9-PHP.B vectors (Figure 4A). We first sought to identify gRNA sequences that could

provide allele-specific targeting of the *Bth* mutation in *Tmc1* (T to A mutation encoding M412K amino acid substitution). Six different 20 nt-long gRNAs were designed with full homology to mouse *Tmc1* mRNA (GenBank: NM\_028953.2) in the region corresponding to nt 1376–1414, which contains the *Bth* mutation (Figure 4B). These gRNAs were chosen to be contiguous to a protospacer adjacent motif (PAM) of SpCas9, corresponding to the canonical NGG sequence for gRNA 11–13 and to the noncanonical NAG sequence for gRNA 14 and 15. In gRNA 21, only the *Bth*-mutated allele carries a noncanonical GAA PAM sequence, which might provide allele-specific targeting.

To identify candidate gRNAs, we screened them for their ability to induce SpCas9 activity at the target *Bth* sequence while preserving the WT allele. Constructs expressing each of the gRNAs and GFP were transfected in diploid mouse embryonic fibroblasts (MEFs) derived from *Bth/+* mice. The MEF cells, previously transduced to constitutively express SpCas9, were sorted for GFP fluorescence and sequenced. To assess the integrity of the gDNA sequence by Sanger sequencing, a PCR amplicon was amplified using primers flanking the *Bth* mutation. As expected, sequencing revealed the presence of the mutation in the *Bth/+* MEF cells, with a mixed A/T signal in position 1398 (Figure 4C). To determine the selectivity of each gRNA, the chromatograms obtained from *Tmc1<sup>+/+</sup>* or *Bth/+* MEF cells were compared to chromatograms from MEF cell cultures transfected with each of the U6-gRNA constructs. The software Tracking of Insertions, Deletions and Recombination Events (TIDER) was used to assess the frequency of the presence of the T nucleotide in position 1398 (Figure 4D).<sup>31</sup> Quantification revealed that only the gRNA 12 and 15 had a significant preference for disrupting the *Bth* allele as compared to the WT allele (Figure 4D). gRNA 15 was selected for further *in vivo* experiments, as it was found to be more selective for the mutated allele than gRNA 12.

Next, we performed a similar analysis using human cells to identify gRNAs displaying similar selectivity for the mutated *TMC1* allele (M418K) in the human genome. In this case, we used two separate human haploid (HAP) cell lines derived from the KBM7 cell line and genetically modified to contain either the WT (HAP *TMC1+*) or the *Bth* *TMC1* genomic sequence (HAP *TMC1Bth*). Both HAP cell lines were transduced for constitutive SpCas9 expression. We designed six different 20 nt-long gRNAs fully homologous to nt 1964–2002 of the human *TMC1* mRNA (GenBank: NM\_138691.3), using a strategy similar to the one previously described for the mouse *Tmc1* sequence (Figure 4B). HAP cells transfected with the U6-gRNA constructs were sorted based on GFP expression. To analyze gDNA integrity, an amplicon containing the *Bth* mutation was amplified for Sanger sequencing. For both HAP *TMC1+* and HAP *TMC1Bth*, we compared chromatograms of both nontransfected and gRNA-transfected cells (Figure 4E). For each gRNA, the presence of insertions and deletions (indels) was analyzed using Tracking of Indels by Decomposition (TIDE) in order to quantify the efficacy of SpCas9-mediated cleavage (Figure 4F).<sup>32</sup> In human HAP cells, gRNA 16 showed clear activity at the *TMC1Bth* allele, whereas no significant in-

del were induced in the WT *TMC1+* HAP cells. However, the gRNA 20, which is the most similar to mouse gRNA 15, showed only low-cleavage efficacy on the *TMC1Bth* allele. Therefore, the gRNA sequence with highest selectivity for the *Bth* mutation appeared to be different in the context of the mouse and human genomes, with gRNA 15 (mouse *Tmc1*) and 16 (human *TMC1*) being the most efficient candidates.

### Dual Vector System for SpCas9/gRNA Targeting the *Bth* Allele Preserves Hearing

Next, we sought to test the efficacy of coinjecting vectors encoding SpCas9 and the gRNA15 into the inner ear of *Bth* mice (*Tmc1<sup>Bth/+</sup>*), a mouse strain that models the progressive hearing loss of DFNA36.<sup>33</sup> To do so, we first packaged each construct into the AAV9-PHP.B capsid: AAV2/9-PHP.B-CMV-SpCas9 (PHP.B-SpCas9) and AAV2/9-PHP.B-U6-gRNA15-CMV-GFP (PHP.B-gRNA15-GFP) to maximize cotransduction efficacy *in vivo*. *Bth* mice were injected through the utricle at P1 with a 1:1 volumetric ratio of viral gRNA15 to SpCas9 (1.35E+11 gc each), and mice were left to recover for at least 4 weeks before testing.

To validate *in vivo* editing specificity, we performed targeted deep sequencing on genomic DNA from whole cochlear tissue of injected *Bth* mice and quantified indel events (Figures S3A and S3B). 30 days after injection, we measured editing efficiency of the *Bth* allele of  $0.6 \pm 0.7\%$  ( $n = 8$ ), which was  $\sim 15$ -fold greater than the editing efficiency of the WT allele,  $0.04 \pm 0.02\%$  ( $n = 8$ ). Since hair cells account for a small fraction of all cells harvested from whole cochleas and since it has been previously demonstrated that PHP.B-EGFP efficiently and almost exclusively transduces IHCs and OHCs,<sup>19</sup> we suspect most of the editing in the cochlea occurred in hair cells. As such, the data suggest high-specificity disruption of the *Bth* allele with negligible activity in the WT allele. Figure S3 examines the allele-specific indel formation of the injected mouse with the highest editing percentage for the *Bth* allele. The indel profile spanning the length of the cochlea reveals that about 95% of CRISPR-induced variants are deletions, with the most frequent being a two-nucleotide deletion in the mutant allele (Figure S3B).

To explore the functional consequences of targeted disruption of the *Bth* allele, ABRs and DPOAEs were recorded from dual-injected *Bth* mice at 4, 6, 12, and 24 weeks following injection. At 4 weeks of age, uninjected *Bth* mice retained decreasing levels of hearing from low to mid frequencies and had little to no detectable ABRs at higher frequencies evoked by up to 110 dB (at 11.3 kHz, 4 weeks:  $54.5 \pm 8.9$  dB,  $n = 7$ ) (Figures 5A and 5B). DPOAEs of *Bth* mice, on average, were only recorded above a 70-dB threshold for all frequencies tested (at 11.3 kHz, 4 weeks:  $71.7 \pm 8.3$  dB,  $n = 7$ ) (Figure 5B). As age increased for *Bth* mice, hearing loss progressed, as seen by increasing ABR thresholds, and by 24 weeks of age, virtually no ABRs or DPOAEs were evoked by up to 110 dB or 80 dB, respectively (Figure 5B). *Bth* mice dual injected with PHP.B-SpCas9 and PHP.B-gRNA15-GFP, on the other hand, retained hearing at low to mid frequencies and was robust up to at least 24 weeks, with low-frequency

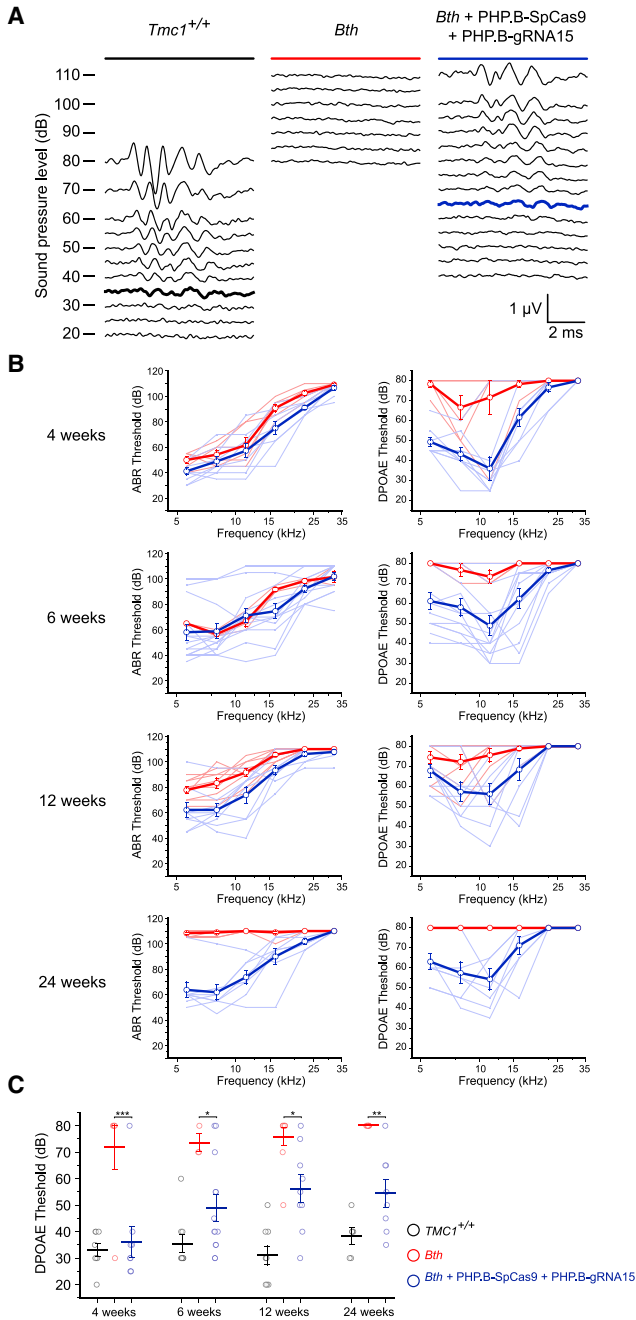


**Figure 5. In Vivo Dual Vector System for SpCas9/gRNA Targeting of the *Bth* Allele**

(A) Representative ABR waveform families recorded from mice at 24 weeks for indicated conditions, using 11.3 kHz tone bursts at incrementally increasing sound-pressure levels. Thresholds were determined by the detection of peak 1 and are indicated by colored traces. Scale bar applies to all families. (B) Mean ABR (left)- and DPOAE (right)-threshold mice plotted as a function of stimulus frequency for *Bth* uninjected controls (red, n = 6 at 4 weeks; n = 3 at 6 weeks; n = 9 at 12 weeks; n = 9 at 24 weeks old) and *Tmc1<sup>Bth/+</sup>* mice dual injected with PHP.B-SpCas9 and PHP.B-gRNA15-GFP (blue, n = 9 at 4 weeks; n = 13 at 6 weeks; n = 9 at 12 weeks; n = 8 at 24 weeks old). Lighter traces show individual responses. Average data shown as

sounds eliciting ABRs at about 60 dB. These results are similar to those observed with single AAV vector injections in *Tmc1<sup>Δ/Δ</sup>* and *Baringo* mice, as well the previous report delivering SaCas9 and gRNA in a single vector<sup>11</sup> (at 11.3 kHz, 4 weeks:  $57.2 \pm 0.4$  dB, n = 9; 6 weeks:  $66.7 \pm 4.4$  dB, n = 13; 12 weeks:  $73.9 \pm 6.3$  dB, n = 9; 24 weeks:  $73.8 \pm 5.2$  dB, n = 8) (Figure 5B). DPOAEs were also significantly recovered at all ages tested, with thresholds returning to WT levels at approximately 35 dB for 11.3 kHz frequencies at 4 weeks of age and elevating to intermediate recovery of about 50 dB at later ages, leveling off when retested at 12 and 24 weeks (at 11.3 kHz, 4 weeks:  $36.1 \pm 5.8$  dB, n = 9; 6 weeks:  $48.8 \pm 4.9$  dB, n = 13; 12 weeks:  $56.1 \pm 5.3$  dB, n = 9; 24 weeks:  $54.4 \pm 5.3$  dB, n = 8) (Figure 5C).

We then asked if hair cell survival also coincided with hearing recovery, as with previous mouse models. As before, we dissected the organ of Corti from cochlea of injected and uninjected *Bth* mice and stained against *Myo7a* to observe hair cell survival and organization. At 24 weeks of age, *Bth* mice have widespread loss of hair cells, with only minimal and disordered cells remaining in apical regions and none toward the middle and basal cochlear turns (for IHCs, apex:  $5.0 \pm 1.5$  cells, middle:  $3.3 \pm 0.7$  cells, and base:  $0 \pm 0$  cells; for OHCs, apex:  $15.7 \pm 4.3$  cells, middle:  $0 \pm 0$  cells, and base:  $0 \pm 0$  cells, n = 3) (Figures 6A and 6B). Dual-injected *Bth* mice, however, have notably greater levels of survival for both IHCs and OHCs at 24 weeks in the apical and middle cochlear turns, whereas hair cell recovery in the basal turn was limited to IHCs (for IHCs, apex:  $8.8 \pm 1.9$  cells, middle:  $8.7 \pm 1.1$  cells, and base:  $4.7 \pm 0.9$  cells; for OHCs, apex:  $31.5 \pm 4.7$  cells, middle:  $10.8 \pm 4.7$  cells, and base:  $2.5 \pm 2.5$  cells, n = 6) (Figures 6A and 6B). This pattern is consistent with the robust rescue of DPOAEs at low to mid frequencies in dual-injected *Bth* mice, whereas the lack of ABRs and DPOAEs detected at high frequencies suggests that IHC survival alone is not sufficient for hearing recovery. To confirm that hearing recovery was correlated to hair cell survival, we plotted the total percentage of surviving IHCs and OHCs combined at sections of each cochlear turn against ABR thresholds at roughly corresponding frequencies, according to a previously reported tonotopic map.<sup>5</sup> By fitting a linear regression, we found that these data were significantly correlated, confirming that rescued hearing broadly correlates with rescued hair cell survival ( $r = 0.624$ ,  $p = 0.013$ ) (Figure 6C).

Because the gRNA15 was packaged with a separate GFP cassette in the same vector, we also imaged GFP expression in dual-injected *Bth* mice and observed that in a best-case scenario, more than 50% of surviving cells also expressed detectable amounts of GFP (Figure 6A). By plotting %GFP+ cells along different cochlear sections against ABR thresholds at corresponding frequencies, we found that a significant linear regression could be fit to these measurements as well ( $r = 0.592$ ;  $p = 0.020$ ) (Figure 6C). Given that dual injection of

mean  $\pm$  SEM. (C) DPOAE thresholds at 11.3 kHz, measured in (B), plotted as a function of age from 4, 6, 12, and 24 weeks (for 4, 6, 12, and 24 weeks, respectively, WT, n = 8, 9, 9, 6; *Tmc1<sup>Bth/+</sup>*, n = 6, 3, 9, 9; dual-injection SpCas9 + gRNA15-GFP, n = 9, 13, 9, 8) (\* $p \leq 0.05$ , \*\* $p \leq 0.01$ , \*\*\* $p \leq 0.001$ ; multiple t tests with Holm-Sidak method). Average data shown as mean  $\pm$  SEM.

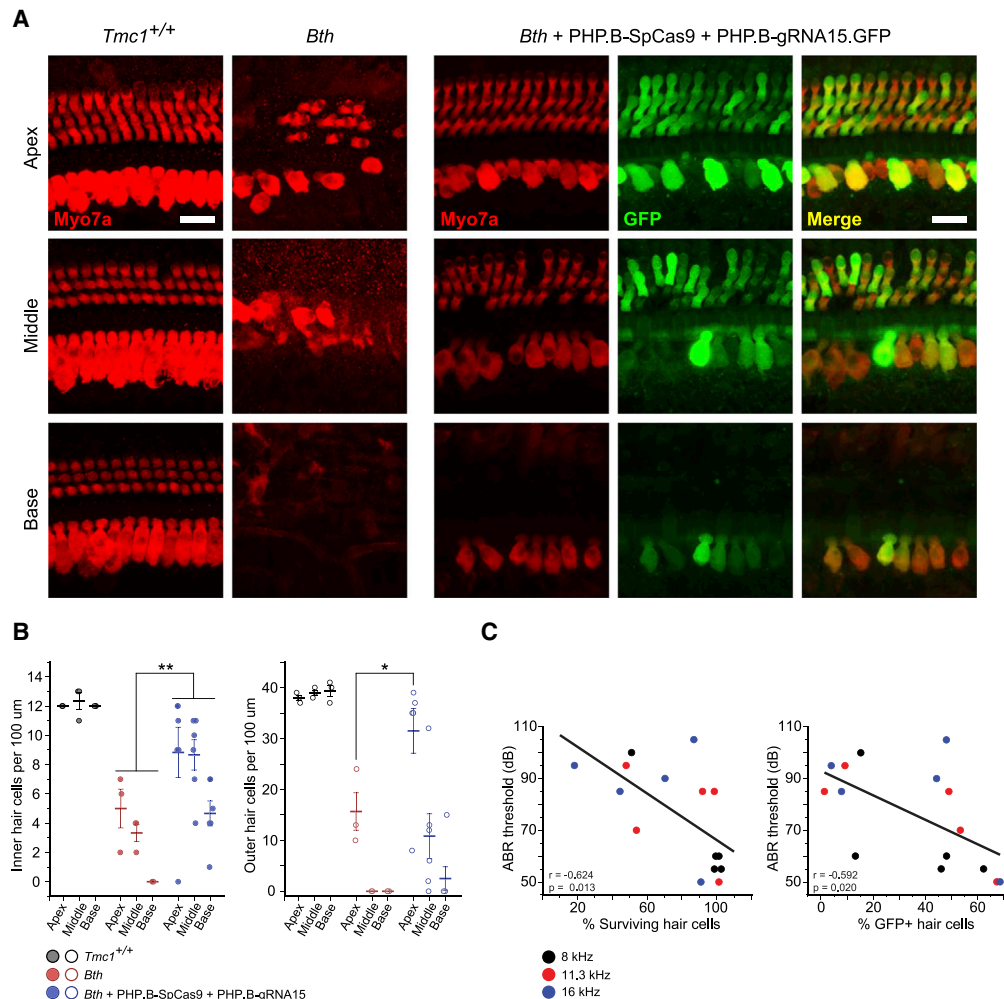


**Figure 6. PHP.B-SpCas9/gRNA Dual Vector Transduction Preserves Hair Cell Survival**

(A) Representative 63 $\times$  confocal images of 100  $\mu$ m sections from the apex, middle, and basal cochlear turns of WT C57BL/6 and uninjected *Tmc1*<sup>Bth/+</sup> mice (right two columns) or *Tmc1*<sup>Bth/+</sup> mice dual injected with PHP.B-SpCas9 and PHP.B-gRNA15-GFP immunostained against myosin VIIa at 24 weeks of age. Scale bar, 20  $\mu$ m. (B) Mean cell counts of IHCs (left) and OHCs (right) for WT C57BL/6 (n = 3), *Bth* uninjected controls (n = 3), and *Bth* mice dual injected with PHP.B-SpCas9 and PHP.B-gRNA15-GFP (n = 6) at 24 weeks of age, measured from 100  $\mu$ m sections of the apex, middle, and basal cochlear turns. Individual samples are shown as a scatterplot (\*\*p  $\leq$  0.01, one-way ANOVA; \*p  $\leq$  0.01, Student's t test). Data shown as mean  $\pm$  SEM. (C) Percentage of surviving hair cells (left) and percentage of GFP-positive hair cells (right) at 24 weeks of age correlated to ABR thresholds measured with 8, 11.3, and 16 kHz tone bursts from *Bth* mice dual injected with PHP.B-SpCas9 and PHP.B-gRNA15-GFP (n = 5 mice; 15 measurements). Data fit with linear regression with  $r = -0.62$  (p = 0.013) for % surviving hair cells and  $r = -0.59$  (p = 0.020) for % GFP+ hair cells.

PHP.B-GFP and PHP.B-RFP yielded a high percentage of coexpressing hair cells, we reasoned that most GFP+ cells from mice dually injected with PHP.B-SpCas9 and PHP.B-gRNA15-GFP had a high likelihood of expressing both constructs as well. Together, these data show that dual vector delivery of SpCas9/gRNA with AAV9-PHP.B can effectively and selectively target the *Bth* allele for nuclease activity and preserve hearing function.

## DISCUSSION

In this study, we demonstrated that efficient gene delivery into hair cells with the synthetic AAV9-PHP.B capsid was able to rescue hearing in three different mouse models for hearing loss. Originally iden-

tified for its dramatically improved CNS tropism and ability to cross the blood brain barrier, AAV9-PHP.B has recently been used successfully in a number of gene-delivery approaches for disease, ranging from synucleinopathy<sup>34</sup> to retinitis pigmentosa.<sup>35</sup> Recently, our group demonstrated that when combined with the CMV promoter and a novel injection route into the inner ear, AAV9-PHP.B also transduces both IHCs and OHCs with higher efficacy than seen with other AAV serotypes.<sup>19</sup> Although prior studies have explored AAV-mediated gene therapy for hereditary hearing loss, they have been met with different limitations to hearing recovery,<sup>5,6,10,20</sup> including variable OHC transduction efficiency with different AAV serotypes, variable experimental conditions, and variability among viral production

facilities.<sup>19,29,36–38</sup> A major advantage of AAV9-PHP.B is its ability to transduce OHCs with the same high efficacy as IHCs, as evidenced by side-by-side comparisons with other AAV serotypes of the same titer and AAV production parameters.<sup>19</sup> Therefore, it is important to characterize the potential for further improved hearing preservation with AAV9-PHP.B.

Gene replacement with PHP.B-Tmc1 in the *Tmc1*<sup>Δ/Δ</sup> model of DFNB7/11 resulted in similar recovery of ABRs compared to a previous report using the AAV-Anc80L65 capsid in the same strain, where near-WT thresholds were observed in the best-performing mice.<sup>5</sup> However, a notable difference that emerged in this study was further improved restoration of DPOAE thresholds over those previously observed, indicating greater recovery of OHC function. OHCs amplify auditory information, and DPOAEs can be used to assess OHC integrity. Therefore, our results are consistent with the notion that improved transduction and subsequent survival of OHCs with PHP.B-Tmc1 resulted in lower DPOAE thresholds, suggesting OHC functional recovery and an improved rescue of hearing sensitivity and frequency discrimination. In some cases, DPOAE thresholds were even lower than those of WT mice, raising the interesting possibility that overexpression of TMC1 may enhance OHC function, possibly through increased TMC1 protein stability or turnover.

Based on our previous report for enhanced transduction of OHCs with PHP.B-EGFP at P7, we explored the potential for increased hearing recovery with injection of PHP.B-Tmc1 at P7 in *Tmc1*<sup>Δ/Δ</sup> mice.<sup>19</sup> Contrary to expectations, ABR thresholds remained high and comparable to results with Anc80L65, and only very modest improvements in DPOAEs were observed in a subset of mice. We therefore tested the efficacy of AAV9-PHP.B gene therapy in *Baringo* mice, which model a recessively inherited sensorineural deafness. *Baringo* mice carry a novel point mutation in *Tmc1* that results in loss of function but are thought to express the TMC1 protein,<sup>23</sup> whereas the *Tmc1*<sup>Δ/Δ</sup> mouse carries a frameshift mutation inducing in premature stop codon and likely no protein product. Taking this into consideration, we proposed that TMC1-Y182C in *Baringo* mice assembles into the macromolecular sensory transduction complex in the stereocilia tips, thus creating a more stable and intact architecture for the incorporation of exogenous functional TMC1 protein, perhaps leading to improved hearing recovery. Indeed, we did see notable improvement in ABRs and especially DPOAEs in a subset of *Baringo* mice injected at P7. However, because the *Baringo* mice were generated in a different background strain, BALB/cJ rather than C57BL/6, it remains possible that improvements observed could be due to innate differences in hair cell integrity or affinity for AAV9-PHP.B. Interestingly, Balb/CJ mice have been reported to have reduced AAV9-PHP.B transduction in the CNS, due to low expression of the *Ly6a* receptor which facilitates AAV9-PHP.B transduction across the blood brain barrier.<sup>39</sup> Presumably, hair cells do not require the *Ly6a* receptor for viral transduction since hair cells of both C57BL/6 and Balb/CJ can be targeted by AAV9-PHP.B with similar efficacy. Non-human primates also lack the *Ly6a* receptor but show robust viral transduction in hair cells with AAV9-PHP.B.<sup>6,21</sup>

The question remains as to why injections at P7 do not recover hearing to the same extent as P1-injected mice, despite similar capacity for viral transduction at both ages. In *Tmc1*<sup>Δ/Δ</sup> mice, P7 injection of PHP.B-EGFP shows that efficient transduction is still possible. Furthermore, IHCs and apical OHCs of P7-injected *Tmc1*<sup>Δ/Δ</sup> mice qualitatively maintain cell survival levels similar to those of P1-injected *Tmc1*<sup>Δ/Δ</sup> mice that recovered a greater extent of hearing. This suggests that hair cell survival is not necessarily an indicator of functional preservation and that the therapeutic window for AAV-mediated gene delivery in *Tmc1* mutant mouse strains may be limited to the first postnatal week. Although *Tmc1* expression in mice begins during the first postnatal week and persists through adulthood,<sup>17</sup> it is possible that trafficking and assembly of sensory transduction occur during a narrow window that limits the efficacy of later introduction of functional TMC1 to the cell. The therapeutic window is likely to be different in humans, as is the progression of hearing onset and loss, which are delayed in patients with *TMC1* mutations relative to mice. Likewise, the *Bth* mouse strain has progressive hearing loss beginning at 1 month of age, whereas DFNA36 patients, who carry similar dominant *TMC1* mutations, begin to lose their hearing in the mid-teen years.<sup>40</sup> Further study is necessary to understand the developmental factors that impact the efficacy of AAV-mediated gene therapy for *Tmc1/TMC1* and other forms of genetic hearing loss.

*Bth* mice cannot be effectively treated with gene replacement due to dominant *Tmc1* mutations, suggesting that the case may be similar for humans with dominant *TMC1* mutations. Alternatively, gene-editing strategies with CRISPR-Cas9-based systems for hearing loss have been explored previously with some success.<sup>11,30</sup> In the current study, AAV9-PHP.B presented the opportunity for dual delivery of two vectors with a smaller chance of decreased efficacy by dilution. We found that by injecting dual AAV9-PHP.B vectors encoding a gRNA and SpCas9 targeting the *Bth* allele, hearing could be preserved with thresholds similar to those of *Tmc1*<sup>Δ/Δ</sup> and *Baringo* mice treated with single AAV9-PHP.B vectors and *Tmc1* gene replacement. For all three mouse models, the rescue of hearing was durable out to 12 weeks postinjection, the latest time point tested.

We noticed that the expression of GFP, indicative of cells transduced with PHP.B-gRNA15-GFP, was variable among cells. Roughly 50% of IHCs and OHCs were GFP positive, substantially less than the near-100% efficacy of single vector PHP.B-GFP transduced alone, seen in our previous study,<sup>19</sup> yet hearing recovery remained as effective as previous single vector experiments. This might suggest that only minimal amounts of transgene expression (less than that needed to produce a detectable GFP signal) are necessary for successful gene editing. It is also possible that a full complement of hair cells may not be needed to recover partial hearing, as detected by ABR and DPOAE thresholds. Alternatively, because gene editing may persist well after the initial injection of the CRISPR-Cas9 system,<sup>11</sup> the 1.1% editing efficiency, measured at 1 month, may have underestimated the number of functional hair cells edited at later stages.

*In vivo* editing efficiency in the current study was comparable to that of other recent gene-editing attempts that targeted the *Bth* allele and reported editing efficiencies of 1.8%<sup>30</sup> and 1.6%.<sup>11</sup> The slightly lower efficiency for the current study may be due to the requirement for dual transduction. Nonetheless, we found the *in vivo* specificity for the *Bth* allele over the WT allele to be ~15-fold, apparently sufficient for preservation of hearing thresholds over the course of this study. However, over the long term, off-target effects that disrupt the WT allele may accumulate and lead to dysfunction. Future studies may focus on the specificity and efficacy of later-stage treatment in progressive hearing-loss models with the improved AAV9-PHP.B capsid delivery.

The level of hearing preservation achieved in this dual vector experiment provides a framework not only for future dual vector studies that require multiple gene-editing elements that cannot be packaged into a single AAV vector but also for dual vector gene replacement of large gene sequences expressed in hair cells and more broadly for gene-therapy approaches in more complicated disease states in which multiple genes may be affected.

In each of the three mouse strains tested in this study, analysis of hair cell survival after injection supports the notion that gene therapy slows or stops the progression of hair cell death in these hearing-loss models. *Tmc1* deficiency interferes with the biophysical maturation of hair cells, characterized by decreased outward K<sup>+</sup> currents, which may lead to the accumulation of intracellular K<sup>+</sup> and ultimately hair cell degeneration.<sup>41</sup> Hair cell death begins from the base and moves toward the apex, and OHCs degenerate faster than IHCs. The efficacy of gene-therapy targeting *Tmc1* may reflect how far along the degenerative pathway cell loss was halted or how soon the native developmental progression was restored by therapeutic intervention. Better understanding of this degenerative path in humans will facilitate development of effective strategies for AAV-mediated inner-ear gene therapy.

In conclusion, we demonstrate that the AAV9-PHP.B capsid is an effective and improved tool for gene delivery in various models of hearing loss. Additionally, its improved efficacy may aid in understanding the biologically relevant pathways that are targeted by AAV-mediated therapy in the inner ear. AAV9-PHP.B is therefore a strong candidate for future clinical applications in treating genetic hearing loss as well as a tool for understanding the basic biology necessary to continue improving gene-therapy tools for inner-ear applications.

## MATERIALS AND METHODS

### Animals

WT mice were C57BL/6J (Jackson Laboratory). For *Tmc1*<sup>Δ/Δ</sup> experiments, mutant mice were of genotype *Tmc1*<sup>Δ/Δ</sup>; *Tmc2*<sup>+/+</sup> on a C57BL/6J background, as previously described.<sup>17</sup> For *Baringo* experiments, genotypes used were: *Tmc1*<sup>Y182C/Y182C</sup>; *Tmc2*<sup>+/+</sup> and *Tmc1*<sup>Y182C/+</sup>; *Tmc2*<sup>+/+</sup> on a BALB/c background, as previously described.<sup>10</sup> The *Tmc1* p.Y182C “*Baringo*” mice were obtained from Murdoch Children’s Research Institute (The Royal Children’s Hospital,

Australia). For *Bth* experiments, mutant mice were of genotype *Tmc1*<sup>Bth/+</sup>; *Tmc2*<sup>+/+</sup> on a C57BL/6J background, as previously described.<sup>33</sup> For all studies, both male and female mice were used in approximately equal proportions. All mice were kept in a 12-h light/12-h dark cycle with food and water *ad libitum*. Mice, ages P1, P7, and P14, were used for *in vivo* delivery of AAV vectors, according to protocols approved by the Institutional Animal Care and Use Committee (protocols #18-01-3610R and #20-02-4149R) at Boston Children’s Hospital (BCH).

### Plasmids and AAV Preparation

For generation of AAV vectors, *Tmc1ex1*, EGFP, and turboRFP were each cloned into the AAV2 vector driven by the CMV promoter and followed with a WPRE site. SpCas9 was cloned into the AAV2 vector driven by CMV without a WPRE site, whereas CMV-GFP and U6-grNA15 were cloned as separate cassettes into the AAV2 vector. AAV vectors were packaged into the AAV9-PHP.B capsid by the Viral Core at BCH and were used under the authority of the BCH Institutional Biosafety Committee (protocol #IBC-P00000447). AAVs were purified by iodixanol gradient ultracentrifuge, followed by ion-exchange chromatography. For injection in *Bth* mice, the vectors were produced at the Bertarelli Foundation Gene Therapy Platform (EPFL; Lausanne, Switzerland). The titers of genome-containing particles were determined for each of the AAV2/9-PHP.B vectors using TaqMan quantitative PCR (qPCR) detecting an amplicon located in the inverted terminal repeats (ITRs), as previously described.<sup>42</sup> Titers were calculated by qPCR with GFP primers (F5′-AGAACGGCATCAAGGTGAAC-3′, R 5′-GAACTCCAGCAGGACCATGT-3′), ITR primers (F 5′-GACCTTTGGTCGCCCCGGCCT-3′, R 5′-GAGTTGGCCACTCCCTCTCTGC-3′), human growth hormone (hGH) primers (F 5′-TGGAAGA CAACCTGTAGGG-3′, R 5′-TGAAACCCCGTCTCTACCAA-3′), or WPRE primers (F 5′-CACTGACAATTCCGTGGTGT-3′, R 5′-GATCCGACTCGTCTGAGG-3′). The titers of each AAV were as follows: AAV2/9-PHP.B-CMV-TMC1ex1-WPRE: 3.91E+13 gc/mL, AAV2/9-PHP.B-CMV-EGFP-WPRE: 1.88E+14 gc/mL, AAV2/9-PHP.B-CMV-turboRFP-WPRE: 2.53E+12 gc/mL, AAV2/9-PHP.B-CMV-SpCas9: 5.4E+14 gc/mL, and AAV2/9-PHP.B-U6-grNA15-CMV-GFP: 5.8E+14 gc/mL. Vectors were aliquoted, stored at –80°C, and thawed immediately prior to use.

### Inner-Ear Utricle Injections

Injections into the utricular vestibule were performed as approved by the Institutional Animal Care and Use Committees at BCH (protocols #18-01-3610R and #17-03-3396R), as previously described.<sup>19</sup> Briefly, mice from P1 to P7 were anesthetized with hypothermia, and older mice were anesthetized with isoflurane. Upon anesthesia, postauricular incision was made to expose the semicircular canals, visualized with a stereo microscope (Zeiss; Stemi 2000). A small puncture was made into the temporal bone surrounding the utricle at the base of the horizontal canal, and injections of 1 μL AAV were performed by inserting a glass micropipette into the puncture site and manually applying light pressure through a syringe. Standard postoperative care was applied after the injection.

## ABR

ABR recordings were performed, as previously described.<sup>5</sup> Mice were anesthetized via intraperitoneal injection with 0.5 mg of ketamine + 0.15 mg xylazine per 10 g body weight. Skin and cartilage that typically obscure the entrance of the external auditory meatus were trimmed away with dissecting scissors, and subcutaneous needle electrodes were inserted at the pinna (active electrode), vertex (reference), and rump (ground). Acoustic stimuli were delivered directly to the studied ear through a custom probe tube speaker/microphone assembly (EPL PXI Systems) consisting of two electrostatic earphones (CUI Miniature Dynamics) to generate primary tones and a Knowles miniature microphone (Electret Condenser) to record ear-canal sound pressure. In a sound-proof chamber, mice were presented 5 ms pure tone stimuli of 5.6, 8, 11.3, 16, 22.6, or 32 kHz at SPLs between 10 and 115 dB in 5 dB steps until a threshold intensity that evoked a reproducible ABR waveform with an identifiable peak 1. With the use of an alternating polarity stimulus, 512 responses were collected and averaged for each SPL. Waveforms with amplitude larger than 15  $\mu$ V (peak to trough) were discarded by an artifact-reject function. Sound pressure at the entrance of the ear canal was calibrated for each individual test subject at all stimulus frequencies. ABR potentials were amplified (10,000 $\times$ ), band-pass filtered (0.3–10 kHz), and digitized using custom data acquisition software (LabVIEW) from the Eaton-Peabody Laboratories Cochlear Function Test Suite. Sound stimuli and electrode voltage were sampled at 40  $\mu$ s intervals using a digital input-output (I-O) board (National Instruments) and stored for offline analysis.

## DPOAEs

DPOAEs were recorded, as previously described, under the same conditions and recording session as for ABRs.<sup>5</sup> Primary tones were produced at a frequency ratio of 1.2 ( $f_2/f_1$ ) for the generation of DPOAEs at  $2f_1-f_2$ , where the  $f_2$  level was 10 dB SPL below  $f_1$  level for each  $f_2/f_1$  pair. The  $f_2$  levels were swept in 10 dB steps from 20 to 80 dB. Waveform and spectral averaging were used at each level to increase the signal-to-noise ratio of the recorded ear-canal sound pressure. The amplitude of the DPOAE at  $2f_1-f_2$  was extracted from the averaged spectra, along with the noise floor at nearby points in the spectrum. Iso-response curves were interpolated from plots of DPOAE amplitude versus sound level. Threshold was defined as the  $f_2$  level required to produce DPOAEs above 0 dB.

## Tissue Dissection and Immunohistochemistry

Temporal bones were dissected, punctured at the round and oval windows and the apical bone, and immersed in 4% paraformaldehyde for 1 h at room temperature for fixation. Temporal bones were then decalcified in 120 mM EDTA for 20 h for 4-week-old mice and up to 1.5 days for 12- and 24-week-old mice. The organ of Corti was micro-dissected in PBS. Tissues were then permeabilized in 0.01% Triton X-100 for 1 h, blocked in 2.5% normal donkey serum and 2.5% bovine serum albumin diluted in PBS (blocking solution) for 1 h, and subsequently stained with a rabbit anti-Myo7a primary antibody (Proteus Biosciences; product #25-6790; 1:500 dilution in blocking solution) at 4°C overnight. Tissues were washed with PBS and then incubated with an anti-rabbit secondary antibody conjugated to Alexa Fluor555

(Life Technologies; 1:200) and phalloidin-Alexa Fluor647 (Molecular Probes; 1:40–1:200) for up to 5 h at room temperature in the dark. Samples were mounted on glass coverslips with Vectashield mounting medium (Vector Laboratories) and imaged at 10 $\times$  or 63 $\times$  magnification using a Zeiss LSM800 confocal microscope. GFP and RFP fluorescence was imaged without additional immunohistochemistry. Image analysis was performed in ImageJ.

## Cloning and Vector Generation for Expression of gRNAs and SpCas9

Original AAV constructs for expression of SpCas9 and gRNA were generously provided by Dr. D. Grimm (Heidelberg University).<sup>43</sup> For SpCas9 expression in cochlear hair cells, we used a pAAV2-CMV-SpCas9 vector. A second pAAV2 vector was used for expression of the individual gRNAs under the control of the U6 promoter. This construct was modified by introducing a RSV-driven GFP-expressing cassette, which was used for the sorting of the transfected cells by fluorescence-activated cell sorting (FACS). The gRNAs for the selective targeting of the mouse and human sequences of *Tmc1* were synthesized (BD Biosciences, UK) and introduced in the gRNA-expressing vector using standard cloning procedures. We used a *trans*-activating CRISPR RNA (tracrRNA), which stabilized the assembly with Cas9, as previously described.<sup>44</sup> The different gRNAs are shown in Figure 4. The lentiviral construct for constitutive expression of SpCas9 in HAP1 and MEF cells was obtained from Addgene (lentiCas9-Blast; #52962) and packaged in vesicular stomatitis virus G protein (VSV-G)-pseudotyped particles using HEK293T cells, according to standard procedures. Vector titer was determined using a p24 ELISA assay (ZeptoMetrix, NY).

## MEF Cell Culture and Transfection

MEFs derived from *Bth/+* mice were grown in Dulbecco's modified Eagle's medium (DMEM; Sigma-Aldrich), supplemented with 10% fetal bovine serum (FBS) and nonessential amino acids (1 $\times$  concentration). The cells were maintained at 37°C as a monolayer in regular culture conditions with 5% CO<sub>2</sub>. *Bth/+* MEF cells were infected with the lentiviral vector encoding SpCas9, and transduced cells were selected in the presence of blasticidin to generate stable lines of SpCas9-expressing cells.

## Analysis of gRNA Efficacy in Mouse *Bth/+* MEF Cells

pAAV2 constructs encoding each of the six different gRNAs were tested for the formation of indels on SpCas9-expressing diploid MEF<sup>*Bth/+*</sup> cells, carrying one copy of each allele. For transfection with the gRNA-expressing constructs, we used Lipofectamine 3000 (Thermo Fisher Scientific) and followed the manufacturer's instructions. After plasmid transfection, gDNA was isolated from GFP-positive MEF cells sorted by FACS. A PCR amplicon was amplified with primers flanking the *Bth* mutation, followed by Sanger sequencing. In order to quantify cleavage efficiency in the Sanger chromatograms, we used the software TIDER.<sup>31</sup> TIDER is a freely accessible web tool to estimate the frequency of nucleotide changes introduced by CRISPR, when using a template DNA allowing for homology-directed repair. Moreover, TIDER provides information regarding the spectrum and

frequency of indels. To determine the cleavage frequency of each gRNA on the WT allele, a +/+ chromatogram was used as control, whereas a *Bth/Bth* chromatogram was used as reference. On the contrary, to assess cleavage frequency on the *Bth* allele, a *Bth/Bth* chromatogram was used as control sample, whereas a +/+ chromatogram was used as reference sample. Results of this analysis were expressed as gRNA efficiency, which reflects for each allele the fraction of the gDNA undergoing Cas9-mediated cleavage. TIDER was used to compare the control sample (nontransfected MEF<sup>Bth/+</sup>-Cas9 cells) with the test samples (MEF<sup>Bth/+</sup>-Cas9 cells transfected with each of the gRNA-expressing constructs).

### Human HAP Cell Line Cell Culture

Human HAP cells carrying the *Bth TMC1* mutation encoding the M418K amino acid substitution were generated from the HAP1 parental cell line, which is derived from the chronic myelogenous leukemia KBM7 cell line (Horizon Genomics, Vienna, Austria).<sup>45</sup> Briefly, a T-to-A point mutation was introduced in exon 16 of the *TMC1* gene (ENSG00000165091; genomic location: chr9: 72,791,914). To insert the mutation by gene editing, the HAP1 cell line was modified with the CRISPR-Cas9 nuclease using gRNA sequences for targeted gDNA cleavage (5'-CAT CGC TTT GAA ATG GCT AC-3' and 5'-AAC CAT GTT CAT CTA CAA GG-3'), and a 1-kb donor template homologous to *TMC1* exon 16 was used to introduce the T-to-A *Bth* mutation. The presence of the mutation was verified by Sanger sequencing of a PCR amplicon. The parental and *Bth* HAP1 cell lines were cultured as a monolayer at 37°C in a humidified atmosphere with 5% CO<sub>2</sub>. As culture medium, we used Iscove's modified Dulbecco's medium (IMDM) plus GlutaMAX (Gibco), supplemented with 10% FBS, 100 U/mL penicillin, and 100 µg/mL streptomycin. Parental and *Bth* HAP1 cells were infected with the lentiviral vector encoding SpCas9, and transduced cells were selected in the presence of blasticidin to generate stable lines of SpCas9-expressing cells.

### Analysis of gRNA Efficacy in Human HAP Cells

Six different gRNAs were tested on human HAP1 cells constitutively expressing Cas9. For transfection, the cells grown in 6-well plates up to 70% confluency were transfected with plasmid DNA using TurboFectin 8.0 (OriGene), following the manufacturer's instructions. 2 days after transfection, the cells were collected for gDNA extraction (NucleoSpin Tissue Kit; Macherey-Nagel AG, Switzerland). gDNA was isolated from GFP-positive cells sorted by FACS, and a PCR was performed with primers flanking the *Bth* mutation, followed by Sanger sequencing. In order to quantify cleavage efficiency by CRISPR-Cas9, the web tool TIDE was used to quantify the formation of indels at a target locus.<sup>32</sup> To determine cleavage frequency, we compared the control sample transfected with the Cas9-expressing plasmid only with test samples cotransfected with the Cas9- and gRNA-expressing plasmids. To assess gRNA cleavage efficiency on WT and *Bth* HAP1 cells, we used as controls chromatograms from either nontransfected WT HAP1 cells or nontransfected *Bth* HAP1 cells, respectively. Results of this analysis were expressed as gRNA efficiency, which reflects the percentage of the gDNA with modifications.

### Mouse Genomic DNA Isolation and Sequencing

Genomic DNA was isolated from injected and uninjected murine cochlear tissue, as previously described.<sup>11</sup> Cochlear tissue was harvested and dissociated with 1 × collagenase I/5 × dispase (Gibco) for 40 min in cell dissociation buffer (Gibco). Organs were further dissociated by passing through a 20G needle, ten times. DNA and RNA from cochlear tissue were isolated using a QIAGEN AllPrep DNA/RNA Micro Kit. To amplify the *Tmc1* gene, we used the following primers: 5'-TAAAGGGACCGCTCTGAAAA-3' (F) and 5'-CCATCAAGGCGAGAATGAAT-3' (R). PCR products were visualized on a 1% agarose gel using and purified on a column (PCR Purification Kit; QIAGEN). CRISPR sequencing was provided by the Massachusetts General Hospital (MGH) DNA Core using 400 ng purified genomic DNA.

### Allele-Specific CRISPResso2 Indel Analysis

To separately analyze CRISPR action on both the *Tmc1Bth* and *Tmc1WT* alleles, FASTQ files were split into read 1 and read 2 and then merged using Flash version (v.)1.2.11, as previously described.<sup>11</sup> The reads from Het samples were segregated based on the presence of WT sequence ("5'-TGGGACAGAACA-3'" and its R complement "5'-TGTTCTGTCCCA-3'") and mutant sequence ("5'-TGGGACAGAACA-3'" and its R complement "5'-AGTTCTGTCCCA-3'"; mutation site is underlined), using a custom Python script (v.3.4.2). Subsequent to segregation, CRISPResso2 was run separately on *Tmc1Bth* and *Tmc1WT* reads with the following parameters: -r1 <fastq\_file> -w 5 -c-ignore\_substitutions <protein\_coding\_sequence> -a <amplicon\_sequence> -g <gRNA\_sequence>.

### SUPPLEMENTAL INFORMATION

Supplemental Information can be found online at <https://doi.org/10.1016/j.ymthe.2020.11.016>.

### ACKNOWLEDGMENTS

Gene-therapy research in the Holt/Geleoc lab is supported by the Jeffrey and Kimberly Barber Fund for Gene Therapy Research, Usher Syndrome Society, and Foundation Pour L'Audition. Work on *Tmc1*<sup>Δ/Δ</sup> and *Baringo* mice was supported by Audition Therapeutics. Work on *Beethoven* mice was supported by the Bertarelli Program in Translational Neuroscience and Neuroengineering and in Switzerland was supported by the Bertarelli Foundation Gene Therapy Platform. This work was supported by the IDDRC (grant 1U54HD090255) and the Neurodevelopmental Behavioral and Viral Cores at Boston Children's Hospital.

### AUTHOR CONTRIBUTIONS

J.W. acquired and analyzed data, generated figures, and wrote the manuscript. P.S. and C.N.-L. acquired and analyzed data and generated figures. S.S., O.S.-O., I.M., and H.G. acquired and analyzed data. B.L.S. acquired funding, generated figures, and helped write the manuscript. J.R.H. conceived the project, acquired funding, and helped write the manuscript.

## DECLARATION OF INTERESTS

J.R.H., P.S., and B.L.S. hold a patent on the use of AAV9-PHP.B for gene therapy in the inner ear. J.R.H. is a scientific founder of Audition Therapeutics and an advisor to several biotech companies focused on inner-ear therapeutics. The authors declare no other competing interests.

## REFERENCES

- Omichi, R., Shibata, S.B., Morton, C.C., and Smith, R.J.H. (2019). Gene therapy for hearing loss. *Hum. Mol. Genet.* 28, R65–R79, R1.
- Smith, R.J.H., Bale, J.F., Jr., and White, K.R. (2005). Sensorineural hearing loss in children. *Lancet* 365, 879–890.
- Marazita, M.L., Ploughman, L.M., Rawlings, B., Remington, E., Arnos, K.S., and Nance, W.E. (1993). Genetic epidemiological studies of early-onset deafness in the U.S. school-age population. *Am. J. Med. Genet.* 46, 486–491.
- Holt, J.R., and Raphael, Y. (2020). Introduction to the Hearing Research special issue on inner ear gene therapy. *Hear. Res.* 394, 108010.
- Nist-Lund, C.A., Pan, B., Patterson, A., Asai, Y., Chen, T., Zhou, W., Zhu, H., Romero, S., Resnik, J., Polley, D.B., et al. (2019). Improved TMC1 gene therapy restores hearing and balance in mice with genetic inner ear disorders. *Nat. Commun.* 10, 236.
- György, B., Meijer, E.J., Ivanchenko, M.V., Tenneson, K., Emond, F., Hanlon, K.S., Indzhykilian, A.A., Volak, A., Karavitaki, K.D., Tamvakologos, P.I., et al. (2018). Gene Transfer with AAV9-PHP.B Rescues Hearing in a Mouse Model of Usher Syndrome 3A and Transduces Hair Cells in a Non-human Primate. *Mol. Ther. Methods Clin. Dev.* 13, 1–13.
- György, B., Sage, C., Indzhykilian, A.A., Scheffer, D.I., Brisson, A.R., Tan, S., Wu, X., Volak, A., Mu, D., Tamvakologos, P.I., et al. (2017). Rescue of Hearing by Gene Delivery to Inner-Ear Hair Cells Using Exosome-Associated AAV. *Mol. Ther.* 25, 379–391.
- Lentz, J.J., Jodelka, F.M., Hinrich, A.J., McCaffrey, K.E., Farris, H.E., Spalitta, M.J., Bazan, N.G., Duelli, D.M., Rigo, F., and Hastings, M.L. (2013). Rescue of hearing and vestibular function by antisense oligonucleotides in a mouse model of human deafness. *Nat. Med.* 19, 345–350.
- Shibata, S.B., Ranum, P.T., Moteki, H., Pan, B., Goodwin, A.T., Goodman, S.S., Abbas, P.J., Holt, J.R., and Smith, R.J.H. (2016). RNA Interference Prevents Autosomal-Dominant Hearing Loss. *Am. J. Hum. Genet.* 98, 1101–1113.
- Yeh, W.H., Shubina-Oleinik, O., Levy, J.M., Pan, B., Newby, G.A., Wornow, M., Burt, R., Chen, J.C., Holt, J.R., and Liu, D.R. (2020). In vivo base editing restores sensory transduction and transiently improves auditory function in a mouse model of recessive deafness. *Sci. Transl. Med.* 12, eaay9101.
- György, B., Nist-Lund, C., Pan, B., Asai, Y., Karavitaki, K.D., Kleinstiver, B.P., Garcia, S.P., Zaborowski, M.P., Solanes, P., Spataro, S., et al. (2019). Allele-specific gene editing prevents deafness in a model of dominant progressive hearing loss. *Nat. Med.* 25, 1123–1130.
- Pan, B., Akyuz, N., Liu, X.-P., Asai, Y., Nist-Lund, C., Kurima, K., Derfler, B.H., György, B., Limapichat, W., Walujkar, S., et al. (2018). TMC1 Forms the Pore of Mechanosensory Transduction Channels in Vertebrate Inner Ear Hair Cells. *Neuron* 99, 736–753.e6.
- Pan, B., Géléoc, G.S., Asai, Y., Horwitz, G.C., Kurima, K., Ishikawa, K., Kawashima, Y., Griffith, A.J., and Holt, J.R. (2013). TMC1 and TMC2 are components of the mechanotransduction channel in hair cells of the mammalian inner ear. *Neuron* 79, 504–515.
- Jia, Y., Zhao, Y., Kusakizako, T., Wang, Y., Pan, C., Zhang, Y., Nureki, O., Hattori, M., and Yan, Z. (2020). TMC1 and TMC2 Proteins Are Pore-Forming Subunits of Mechanosensitive Ion Channels. *Neuron* 105, 310–321.e3.
- Imtiaz, A., Maqsood, A., Rehman, A.U., Morell, R.J., Holt, J.R., Friedman, T.B., and Naz, S. (2016). Recessive mutations of TMC1 associated with moderate to severe hearing loss. *Neurogenetics* 17, 115–123.
- Sloan-Heggen, C.M., Bierer, A.O., Shearer, A.E., Kolbe, D.L., Nishimura, C.J., Frees, K.L., Ephraim, S.S., Shibata, S.B., Booth, K.T., Campbell, C.A., et al. (2016). Comprehensive genetic testing in the clinical evaluation of 1119 patients with hearing loss. *Hum. Genet.* 135, 441–450.
- Kawashima, Y., Géléoc, G.S., Kurima, K., Labay, V., Lelli, A., Asai, Y., Makishima, T., Wu, D.K., Della Santina, C.C., Holt, J.R., and Griffith, A.J. (2011). Mechanotransduction in mouse inner ear hair cells requires transmembrane channel-like genes. *J. Clin. Invest.* 121, 4796–4809.
- Deverman, B.E., Pravdo, P.L., Simpson, B.P., Kumar, S.R., Chan, K.Y., Banerjee, A., Wu, W.L., Yang, B., Huber, N., Pasca, S.P., and Gradinaru, V. (2016). Cre-dependent selection yields AAV variants for widespread gene transfer to the adult brain. *Nat. Biotechnol.* 34, 204–209.
- Lee, J., Nist-Lund, C., Solanes, P., Goldberg, H., Wu, J., Pan, B., Schneider, B.L., and Holt, J.R. (2020). Efficient viral transduction in mouse inner ear hair cells with utricle injection and AAV9-PHP.B. *Hear. Res.* 394, 107882.
- Askew, C., Rochat, C., Pan, B., Asai, Y., Ahmed, H., Child, E., Schneider, B.L., Aebischer, P., and Holt, J.R. (2015). Tmc gene therapy restores auditory function in deaf mice. *Sci. Transl. Med.* 7, 295ra108.
- Ivanchenko, M.V., Hanlon, K.S., Devine, M.K., Tenneson, K., Emond, F., Lafond, J.F., Kenna, M.A., Corey, D.P., and Maguire, C.A. (2020). Preclinical testing of AAV9-PHP.B for transgene expression in the non-human primate cochlea. *Hear. Res.* 394, 107930.
- Akil, O., Dyka, F., Calvet, C., Emptoz, A., Lahlou, G., Nouaille, S., Boutet de Monvel, J., Hardelin, J.P., Hauswirth, W.W., Avan, P., et al. (2019). Dual AAV-mediated gene therapy restores hearing in a DFN9 mouse model. *Proc. Natl. Acad. Sci. USA* 116, 4496–4501.
- Manji, S.S., Miller, K.A., Williams, L.H., and Dahl, H.H. (2012). Identification of three novel hearing loss mouse strains with mutations in the Tmc1 gene. *Am. J. Pathol.* 180, 1560–1569.
- Holt, J.R., and Geleoc, G.S. (2019). Split otoferlins reunited. *EMBO Mol. Med.* 11, e9995.
- Akil, O. (2020). Dual and triple AAV delivery of large therapeutic gene sequences into the inner ear. *Hear. Res.* 394, 107912.
- Reisinger, E. (2020). Dual-AAV delivery of large gene sequences to the inner ear. *Hear. Res.* 394, 107857.
- Amoasii, L., Long, C., Li, H., Mireault, A.A., Shelton, J.M., Sanchez-Ortiz, E., McAnally, J.R., Bhattacharyya, S., Schmidt, F., Grimm, D., et al. (2017). Single-cut genome editing restores dystrophin expression in a new mouse model of muscular dystrophy. *Sci. Transl. Med.* 9, eaan8081.
- Al-Moyed, H., Cepeda, A.P., Jung, S., Moser, T., Kügler, S., and Reisinger, E. (2019). A dual-AAV approach restores fast exocytosis and partially rescues auditory function in deaf otoferlin knock-out mice. *EMBO Mol. Med.* 11, e9396.
- Omichi, R., Yoshimura, H., Shibata, S.B., Vandenberghe, L.H., and Smith, R.J.H. (2020). Hair Cell Transduction Efficiency of Single- and Dual-AAV Serotypes in Adult Murine Cochleae. *Mol. Ther. Methods Clin. Dev.* 17, 1167–1177.
- Gao, X., Tao, Y., Lamas, V., Huang, M., Yeh, W.H., Pan, B., Hu, Y.J., Hu, J.H., Thompson, D.B., Shu, Y., et al. (2018). Treatment of autosomal dominant hearing loss by in vivo delivery of genome editing agents. *Nature* 553, 217–221.
- Brinkman, E.K., Kousholt, A.N., Harmsen, T., Leemans, C., Chen, T., Jonkers, J., and van Steensel, B. (2018). Easy quantification of template-directed CRISPR/Cas9 editing. *Nucleic Acids Res.* 46, e58.
- Brinkman, E.K., Chen, T., Amendola, M., and van Steensel, B. (2014). Easy quantitative assessment of genome editing by sequence trace decomposition. *Nucleic Acids Res.* 42, e168.
- Vreugde, S., Erven, A., Kros, C.J., Marcotti, W., Fuchs, H., Kurima, K., Wilcox, E.R., Friedman, T.B., Griffith, A.J., Balling, R., et al. (2002). Beethoven, a mouse model for dominant, progressive hearing loss DFNA36. *Nat. Genet.* 30, 257–258.
- Morabito, G., Giannelli, S.G., Ordazzo, G., Bido, S., Castoldi, V., Indrigo, M., Cabassi, T., Cattaneo, S., Luoni, M., Cancellieri, C., et al. (2017). AAV-PHP.B-Mediated Global-Scale Expression in the Mouse Nervous System Enables GBA1 Gene Therapy for Wide Protection from Synucleinopathy. *Mol. Ther.* 25, 2727–2742.
- Giannelli, S.G., Luoni, M., Castoldi, V., Massimino, L., Cabassi, T., Angeloni, D., Demontis, G.C., Leocani, L., Andreazzoli, M., and Broccoli, V. (2018). Cas9/sgRNA

- selective targeting of the P23H Rhodopsin mutant allele for treating retinitis pigmentosa by intravitreal AAV9.PHP.B-based delivery. *Hum. Mol. Genet.* 27, 761–779.
36. Ayuso, E., Blouin, V., Lock, M., McGorray, S., Leon, X., Alvira, M.R., Auricchio, A., Bucher, S., Chtarto, A., Clark, K.R., et al. (2014). Manufacturing and characterization of a recombinant adeno-associated virus type 8 reference standard material. *Hum. Gene Ther.* 25, 977–987.
  37. Landegger, L.D., Pan, B., Askew, C., Wassmer, S.J., Gluck, S.D., Galvin, A., Taylor, R., Forge, A., Stankovic, K.M., Holt, J.R., and Vandenberghe, L.H. (2017). A synthetic AAV vector enables safe and efficient gene transfer to the mammalian inner ear. *Nat. Biotechnol.* 35, 280–284.
  38. Isgrig, K., McDougald, D.S., Zhu, J., Wang, H.J., Bennett, J., and Chien, W.W. (2019). AAV2.7m8 is a powerful viral vector for inner ear gene therapy. *Nat. Commun.* 10, 427.
  39. Huang, Q., Chan, K.Y., Tobey, I.G., Chan, Y.A., Poterba, T., Boutros, C.L., Balazs, A.B., Daneman, R., Bloom, J.M., Seed, C., and Deverman, B.E. (2019). Delivering genes across the blood-brain barrier: LY6A, a novel cellular receptor for AAV-PHP.B capsids. *PLoS ONE* 14, e0225206.
  40. Zhao, Y., Wang, D., Zong, L., Zhao, F., Guan, L., Zhang, P., Shi, W., Lan, L., Wang, H., Li, Q., et al. (2014). A novel DFNA36 mutation in TMC1 orthologous to the Beethoven (Bth) mouse associated with autosomal dominant hearing loss in a Chinese family. *PLoS ONE* 9, e97064.
  41. Marcotti, W., Erven, A., Johnson, S.L., Steel, K.P., and Kros, C.J. (2006). Tmc1 is necessary for normal functional maturation and survival of inner and outer hair cells in the mouse cochlea. *J. Physiol.* 574, 677–698.
  42. D'Costa, S., Blouin, V., Broucque, F., Penaud-Budloo, M., François, A., Perez, I.C., Le Bec, C., Moullier, P., Snyder, R.O., and Ayuso, E. (2016). Practical utilization of recombinant AAV vector reference standards: focus on vector genomes titration by free ITR qPCR. *Mol. Ther. Methods Clin. Dev.* 5, 16019.
  43. Schmidt, F., and Grimm, D. (2015). CRISPR genome engineering and viral gene delivery: a case of mutual attraction. *Biotechnol. J.* 10, 258–272.
  44. Chen, B., Gilbert, L.A., Cimini, B.A., Schnitzbauer, J., Zhang, W., Li, G.W., Park, J., Blackburn, E.H., Weissman, J.S., Qi, L.S., and Huang, B. (2013). Dynamic imaging of genomic loci in living human cells by an optimized CRISPR/Cas system. *Cell* 155, 1479–1491.
  45. Kotecki, M., Reddy, P.S., and Cochran, B.H. (1999). Isolation and characterization of a near-haploid human cell line. *Exp. Cell Res.* 252, 273–280.